Journal of Materials Chemistry C

FEATURE ARTICLE

Cite this: J. Mater. Chem. C, 2014, 2, 7460

Optical sensing of biological, chemical and ionic species through aggregation of plasmonic nanoparticles

Lakshminarayana Polavarapu,*[ab] Jorge Pérez-Juste,*[a] Qing-Hua Xu*[c] and Luis M. Liz-Marzán*[abd]

Plasmonic nanoparticles made of gold and silver have attracted a great deal of research attention in various fields, such as biosensors, imaging, therapy, nanophotonics, catalysis and light harvesting due to their unique optical and electronic properties. Plasmonic nanoparticle colloids may exhibit strong colours in the visible region due to localized surface plasmon resonances, whereas their aggregates exhibit different linear and nonlinear optical properties. Therefore, a smart design of chemical interactions between analytes and the nanoparticles surface may lead to gradual optical changes, which can be probed by various sensing methods, allowing quantitative analyte detection. A significant amount of research has been carried out toward the development of plasmonic sensors based on analyte-induced aggregation of Au or Ag nanoparticles, and the sensitivity and selectivity of such plasmonic biosensors have been greatly improved over the years. In this feature article, we summarize different design strategies that have been employed to induce the aggregation of plasmonic nanoparticles upon the addition of various analytes such as DNA, proteins, organic molecules and inorganic ions. We introduce various optical assays, such as colorimetry, surface-enhanced Raman scattering, two-photon photoluminescence, dynamic light scattering, hyper-Rayleigh scattering and chiroptical activity. From the discussion, it can be concluded that plasmonic sensors based on nanoparticle aggregation offer simple, highly sensitive and selective detection of various analytes. Finally, we discuss some of the future directions of plasmonic nanosensors toward device integration for practical applications.

Received 31st May 2014
Accepted 11th July 2014

DOI: 10.1039/c4tc01142b

www.rsc.org/MaterialsC

[a]Departamento de Química Física, Universidade de Vigo, 36310 Vigo. E-mail: lakshmi@uvigo.es; juste@uvigo.es

[b]Bionanoplasmonics Laboratory, CIC biomaGUNE, Paseo de Miramón 182, 20009 Donostia – San Sebastián, Spain. E-mail: llizmarzan@cicbiomagune.es

[c]Department of Chemistry, National University of Singapore, 3 Science Drive 3, Singapore 117543. E-mail: chmxqh@nus.edu.sg

[d]Ikerbasque, Basque Foundation for Science, 48011 Bilbao, Spain

Lakshminarayana obtained his Masters degree from the University of Hyderabad (India) in 2005 and his PhD degree from the National University of Singapore (Singapore) in 2011. He worked as a postdoctoral fellow CIC biomaGUNE in San Sebastián (2012–2013), and he is currently a postdoctoral fellow at University of Vigo (Spain). He is a co-author of over 30 publications and his current research interests include the design and fabrication of plasmonic substrates for SERS- and LSPR-based sensing applications.

Jorge Pérez-Juste obtained his Chemistry degree from the Universidade de Santiago de Compostela in 1995 and his PhD degree in Chemistry from the Universidade de Vigo in 1999. He worked as a postdoctoral fellow at UCSC in 2000 and at University of Melbourne (Australia) in 2002 and 2003. Since 2009, he has been an Associate Professor at the University of Vigo. His current interests include the synthesis and assembly of nanoparticles and nanostructured materials with tailored optical and sensing properties.

1. Introduction

Biological, chemical and ion sensors have become crucial in improving health and environment by the early detection of diseases and by continuous monitoring of toxic chemicals or ions that are threats to environmental safety. Water pollution is an example of global issues leading to sickness of millions of people all around the world. Due to the industrial expansion, tons of toxic chemicals, including pesticides and heavy metal ions, are expelled into our environment every day, causing serious problems to human health *via* the food chain and exposure from breathing air.[1,2] Various types of traditional sensors, such as gas/liquid chromatography,[3] mass spectrometry[4] and atomic absorption spectroscopy[5] have been widely applied for continuous monitoring of water, and a variety of chemical sensors, biomarkers and capillary-based sequencing, PCR, and multiplex ligation-dependent probe amplification techniques have often been utilized in hospitals for DNA-based testing and molecular diagnosis of diseases.[6–8] Although these analytical techniques provide accurate quantitative detection, they require complex instrumentation, thereby becoming expensive and time consuming. After the emergence of nanotechnology in the 20th century, nanomaterials including metals, semiconductors, polymers, carbon nanotubes and graphene have played a significant role in the field of analytical chemistry by providing simple and cost-effective solutions for various types of sensors.[9–11]

Among all, nanoparticles (NPs) of noble metals, such as Au and Ag have attracted research around the development of simple, efficient, portable, point of care detection and cost-effective sensors based on their optical and electronic properties.[12–17] Au and Ag NPs exhibit strong localized surface plasmon resonances (LSPR), which arise from the collective oscillations of conduction band electrons induced by the interaction of electromagnetic radiations.[18] The LSPR frequencies of Au and Ag NPs depend on their morphology, interparticle distance and the refractive index of the surrounding medium.[15,18,19] Plasmonic NPs have an ability to concentrate light at the nanometer scale by producing strong field enhancement through the excitation of their LSPR, rendering them attractive in various applications, such as chemical and biological sensing, imaging, therapy, photonics and plasmon-enhanced light harvesting.[10] The local electromagnetic fields near the nanostructure surface can be several orders of magnitude higher than the incident field, resulting in very strong scattering of the incident field at the LSPR wavelength.[19] Field enhancements by plasmonic NPs have been utilized for various so-called plasmon-enhanced optical phenomena, such as surface-enhanced Raman scattering (SERS),[20] metal-enhanced fluorescence,[21] or plasmonic photocatalysis.[22]

SERS in particular has become a powerful spectroscopy technique for the ultrasensitive detection and quantification of a variety of analytes ranging from ions and small molecules to large proteins.[20] SERS is based on the detection of amplified Raman scattering of analyte molecules at low concentrations, when they are in close proximity to a plasmon-excited nanostructured metallic surface. An alternative type of sensing is based on the LSPR sensitivity of plasmonic nanostructures, with respect to the refractive index of the surrounding molecular environment.[23] LSPR-based sensing has been extensively discussed in many earlier review articles by several researchers and therefore has been excluded from the content of the present feature article.[23,24] On the other hand, the absorption and scattering coefficients of plasmonic nanoparticles are several orders of magnitude higher than those of conventional organic dyes, and therefore they exhibit intense colours in the visible region, which makes them suitable for naked-eye detection of analytes that induce colour changes through the aggregation of nanoparticles. The high scattering ability of plasmonic NPs has opened various ways toward different scattering based sensing

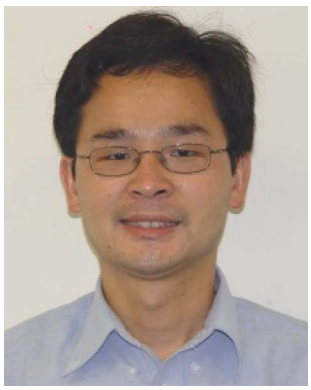

Qing-Hua Xu obtained his BS degree from Zhejiang University (1993), MS degrees from Peking University (1996) and University of Chicago (1997), and PhD degree from UC Berkeley (2001). He conducted his postdoctoral research at Stanford University (2001–2002) and UC Santa Barbara (2002–2005). He joined the Department of Chemistry, National University of Singapore, as an Assistant Professor in 2005 and has been an Associate Professor of the same university since 2011. He is a co-author of over 100 peer-reviewed publications. His current research interests include linear and nonlinear optical properties of nanocomposite materials and their applications in imaging, sensing, biomedicine and energy areas.

Luis M. Liz-Marzán is a PhD from the University of Santiago de Compostela (1992) and has been a postdoc at Utrecht University and (more recently) a visiting professor at Tohoku University, Michigan, Melbourne, Hamburg and Max-Planck Institute Golm. He has been a Professor in Physical Chemistry at the University of Vigo (1995–2012), and he is currently an Ikerbasque Research Professor and Scientific Director of CIC biomaGUNE in San Sebastián. He is a co-author of over 350 publications and 5 patents, and has received several research awards. His current interests include nanoparticle synthesis and assembly, nanoplasmonics, and development of nanoparticle-based sensing and diagnostic tools.

methods, such as dynamic light scattering (DLS)[25] or hyper-Rayleigh scattering (HRS),[26] for optical detection. In addition, other optical effects, such as two-photon photoluminescence (TPPL)[27] and chiroptical activity[28] of nanostructures have also been investigated for optical sensing. Interestingly, all of the above mentioned properties of plasmonic nanostructures exhibit significant enhancements when they are aggregated, as compared to the individual components, due to interparticle plasmon coupling. Therefore, a clever design of chemical interactions between analytes and NPs surfaces that would result in aggregation can be optically probed by simply measuring scattering signals with respect to analyte concentration. In this feature article, we summarize the design of plasmonic sensors based on the aggregation of Au and Ag NPs, and we also discuss different detection methods, such as colorimetric, SERS, DLS, TPPL, HRS and chiroptical activity, which have been applied for the sensing of biomolecules such as DNA, proteins and amino acids, small molecules and inorganic ions.

2. Surface plasmon coupling in aggregated plasmonic NPs and application to sensing

Surface plasmon resonance coupling is an important phenomenon in the field of plasmonics, which arises when two or more adjacent NPs of the same or different morphology are in close contact.[15,18,19,29–32] Such LSPR coupling may allow us, for example, to construct optical circuits, in which light can be guided, modulated and harvested on sub-micron length scales.[33–35] Coupled plasmonic NPs may also exhibit completely different and even enhanced linear and nonlinear optical properties.[36,37] Therefore, various strategies have been implemented for the directed self-assembly of plasmonic nanostructures to achieve control over their optical and electronic properties for desired applications.[30,38–40] In addition, the near field enhancement at the gap between coupled NPs is several orders of magnitude higher than at the individual particles; therefore, such gaps are usually called "hot spots".[19,41] Aggregated plasmonic NPs typically exhibit LSPR band redshift and broadening, the extent of such shifts depending on the strength of plasmon coupling,[31] which in turn is determined by the distance and angle between the adjacent NPs as has been verified by Link *et al.*[42] for nanoparticle chains, and by Huang *et al.*[43] for spherical dimers. Recently, Mulvaney *et al.* reported the surface plasmon resonances of strongly coupled gold nanosphere chains from monomer to hexamer, with interparticle spacings of 1 nm, where a continuous red shift was observed with increasing chain length, which was mainly due to dipole–dipole coupling.[44] On the other hand, three-dimensional (3D) spherical symmetric aggregates exhibit different spectral shifts compared to linear aggregates. For instance, Pazos-Pérez *et al.*[45] reported the optical properties of highly symmetrical Au nanoparticle aggregates with coordination numbers up to 7. They observed an LSPR redshift for dimers and then blue shifts together with spectral broadening as the coordination number was increased, which also caused an increase of SERS enhancement factor. In another report, Halas *et al.* showed that the optical properties of 3D plasmonic aggregates can be highly sensitive to particle number and cluster geometry.[46] Similar to spherical plasmonic NPs, anisotropic nanostructures, such as Au nanoshells also exhibit dramatically different optical properties when they aggregate, as reported by Halas *et al.*[47] The plasmon coupling between aggregated NPs can be viewed as the hybridization of their individual plasmon modes, in analogy to the linear combinations of atomic orbitals in molecular orbital theory, as proposed by Nordlander *et al.*[48,49] In this model, the plasmon modes of interacting NPs hybridize either in-phase or out-of-phase, leading to the formation of a lower energy bonding mode or a higher energy antibonding plasmon mode, respectively (Fig. 1a). The in-phase and out-of-phase combinations reflect the bonding (σ) and antibonding (σ^*) modes, if the incident polarization is along the longitudinal axis of a dimer. While the bonding mode leads to electric field enhancement at the junction within the dimer and redshift of LSPR frequency, the antibonding mode leads to the localization of electric fields at the ends of the dimer and blue shift of LSPR frequency. The situation reverses when the incident polarization is transverse, meaning that the in-phase mode reflects the antibonding mode (π^*) and the out-of-phase reflects the bonding mode (π). However, the plasmon coupling and LSPR shifts are weaker in the case of transverse polarization. It should be noted that the out-of-phase modes do not exist in homodimers due to the cancellation of equal but oppositely oriented dipoles on two particles. This plasmon hybridization model has been well accepted by the scientific community and has been applied to explain the plasmonic properties of various nanostructures, such as Au/Ag homo and heterodimers, nanostars and nanoshells.[48,50–53] The existing theoretical and experimental studies tell us that the optical properties (colour change and LSPR shift) of coupled NPs depend on whether the aggregates are spherical or nonspherical.[18,30,32,54,55] In general, the suspensions of spherical Au NPs (10–50 nm diameter) display a ruby red colour, while aggregates exhibit purple or blue colours.[16,56] On the other hand, the colour of Ag NPs changes from yellow to brown, orange and green when they aggregate,[16] and the resulting

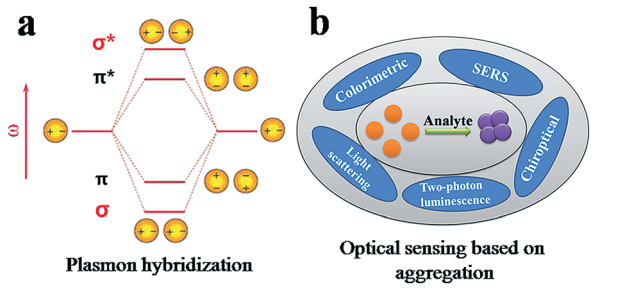

Fig. 1 (a) Plasmon hybridization model in a nanoparticle dimer. The plasmon modes of interacting nanoparticles can be expressed as a linear combination of their individual plasmon modes, in analogy to molecular orbital theory. (b) Different types of optical sensing methods based on aggregation of plasmonic NPs. (Panel a reproduced with permission from ref. 53.)

colour depends on interparticle distance and NPs size. Thus, one can design colorimetric plasmonic sensors in such a way that analyte molecules or ions induce aggregation of plasmonic NPs through electrostatic interactions or hydrogen bonding.[13,14,16,17,56–61] This colorimetric detection is rapid, simple and portable.[62] However, it is difficult to implement a quantitative determination of the analyte by naked-eye observation.

In addition, aggregated plasmonic NPs exhibit enhanced scattering due to increase of particle size, which makes them suitable for scattering based sensing.[20,63,64] For instance, the SERS efficiency increases with the extent of aggregation due to the increased formation of hot spots.[41,45,65] Because the scattering enhancement depends on the extent of aggregation, one can in principle monitor such an enhancement with respect to analyte concentration for quantitative determination.[58,63] In addition to SERS, we discuss different types of assays that have been implemented in the literature with more detail in the following sections (Fig. 1b). Although the signal detection mechanisms are different in different assays, the basic design of analyte-induced aggregation is common in all the detection methodologies presented in this feature article.

3. Colorimetric sensing

Plasmonic colorimetric assays are based on the colour change that occurs in NP solutions when they switch from individual into aggregated states, mediated by the selective action of certain analytes.[14,16,17,56–58,60,61] The high extinction cross section of Au and Ag NPs in the visible renders them suitable for colorimetric assays, even based on naked-eye detection. The detection method is thus instrumentation free, simple, sensitive, selective, rapid, portable and applicable to a wide range of analytes, related to biological, clinical, food and environmental safety.[14,16,17,56–58,60,61,66] In particular, the colorimetric detection of DNA using Au NPs by Mirkin *et al.*[67] has revolutionized the field of plasmonic colorimetric sensors. After this pioneering work,

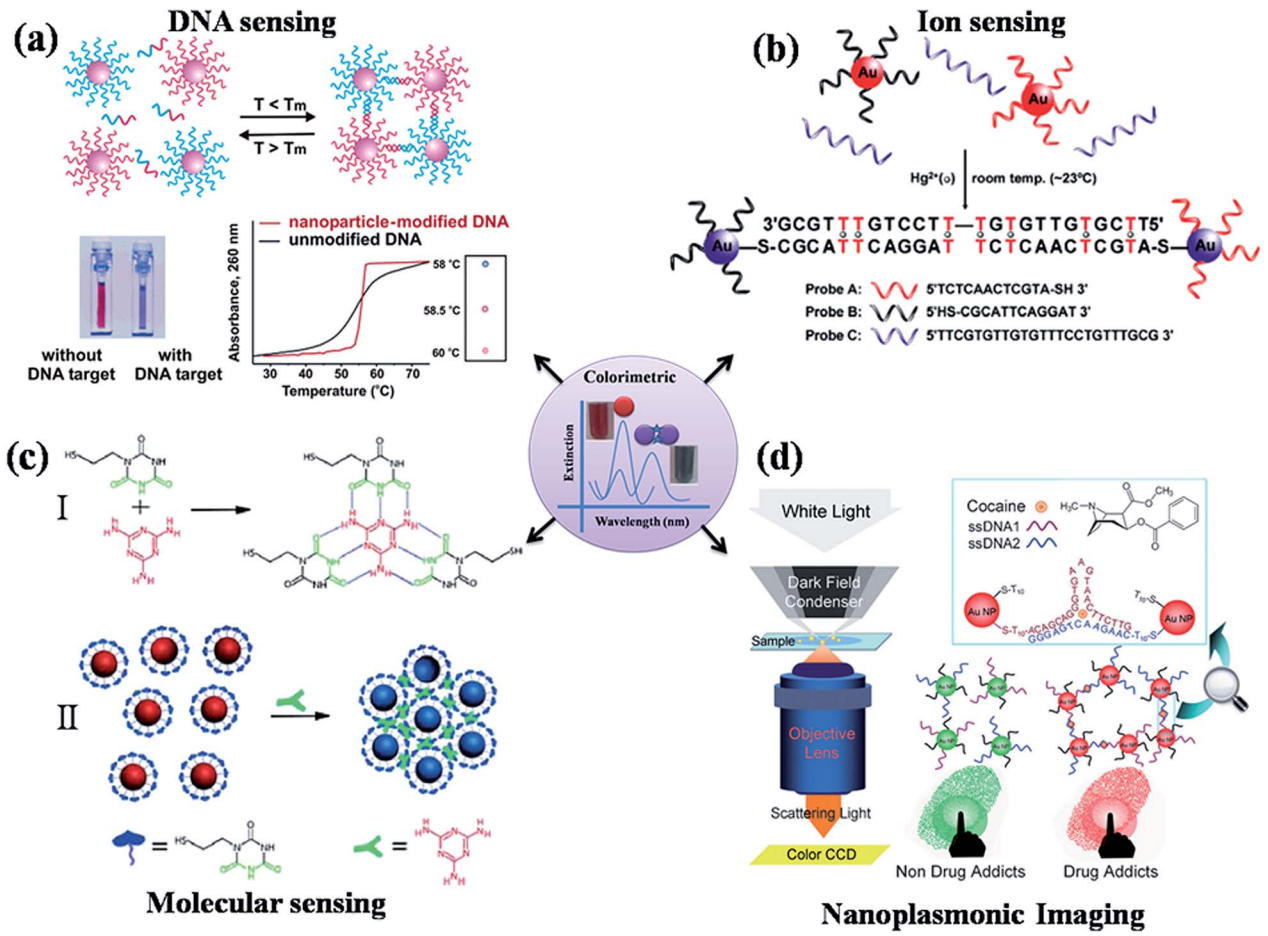

Fig. 2 Colorimetric sensing: (a) schematic representation of a strategy for colorimetric DNA detection using DNA conjugated Au NPs. The addition of a complementary target to DNA oligonucleotide-functionalized gold nanoparticles leads to aggregation, resulting in a change of solution colour from red to blue. The aggregation process can also be monitored by UV-visible spectroscopy at different temperatures. (b) Colorimetric sensing of Hg^{2+} using T-DNA conjugated Au NPs through T–Hg^{2+}–T complexation. (c) Visual detection of melamine using MTT-stabilized gold nanoparticles (II) *via* H-bonding recognition between melamine and a cyanuric acid derivative (I). (d) Strategy for nanoplasmonic imaging of latent fingerprints (LFPs) and identification of cocaine in LFPs by dark-field microscopy using DNA conjugated Au NPs. Here, cocaine acts as a molecular linker to aggregate the DNA conjugated Au NPs probes (Panels a, b, c and d reproduced with permission from ref. 14, 102, 86 and 91, respectively).

the approach has been exploited for the detection of different kinds of DNA,[68–82] RNA,[83,84] proteins,[85] cancerous cells,[66] organic molecules[70,86–93] and metal ions[94–102] (Fig. 2). In this section, we review advancements in the colorimetric detection of various analytes using different design strategies with selectivity and improved sensitivity. Most of the examples covered in this section will be based on the aggregation of Au NPs as it has been shown that they are not only inert, but also exhibit colours that the human eye is more sensitive to, but their surface chemistry also allows specific chemical design to facilitate the aggregation by the addition of specific analytes.

The first breakthrough reports on the assembly of nanocrystals using DNA was independently reported in 1996 by Mirkin *et al.*[67] and Alivisatos *et al.*[103] In their studies, gold nanocrystal surfaces were first modified with thiolated DNA and then a complementary DNA strand induced the aggregation of NPs *via* a DNA double strand, leading to a colour change from red to blue, which can be accurately monitored by UV-visible spectroscopy (Fig. 2a).[14,67] Based on this first discovery, Mirkin *et al.* and others reported various kinds of Au NP biomarkers by modifying the NPs surface with different kinds of thiolated DNA strands.[73,75,76,81,104] Using this method, one can selectively differentiate the type of DNA, even if only with a single base pair mismatch, as reported by Storhoff *et al.*[76] An additional advantage of such a simple method is that it can be applied on solid substrates for chip-based detection.[80,81] For example, Taton *et al.*[81] reported scanning DNA array detection using DNA modified Au NP probes on glass substrates, and the sensitivity was further improved by catalytic reduction of Ag^+ ions on the immobilized gold NPs surface. Despite several advantages, one drawback of this colorimetric detection method is its relatively low sensitivity and narrow dynamic range in solution. This was overcome by Chen *et al.*,[72] who demonstrated DNA optical sensing through DNA-functionalized AuNP dimers immobilized on a substrate. In addition, Zhao *et al.*[105] showed that the colorimetric sensitivity could be improved when the aggregation was performed on a bright background provided by paper, on which the colour change could be easily observed. Anisotropic nanostructures, such as gold nanorods have also been used to improve the sensitivity of DNA detection by Ma *et al.*[69] In a recent report, Guo *et al.*[73] showed that the oriented aggregation of Au NPs could significantly improve DNA detection sensitivity. In their approach, nanoparticles were asymmetrically functionalized with PEG and DNA, so that a limited amount of DNA binds to only one side of the NPs surface, so as to obtain dimers upon the addition of target DNA. Moreover, they showed that the distance between the nanoparticles could be minimized through the formation of a Y-shaped DNA duplex, which improved the limit of detection by 10^4 times.[73]

In addition to colorimetric DNA detection using DNA modified Au NPs as discussed above, several research groups have demonstrated DNA detection using unmodified Au NPs (label-free approach), which avoids DNA labeling.[77,78,106] For example, Li and Rothberg have shown that single-stranded DNA protects unmodified gold nanoparticles from aggregation at high ionic strength through electrostatic interactions, whereas double-stranded DNA does not, thus allowing DNA detection through colour change.[77] They have also shown that <100 femtomoles of target DNA can be detected through color changes and even single-base-pair mismatches can be readily detected. A more universal biosensor approach for the colorimetric detection of DNA, small molecules, proteins and ions using unmodified Au NPs and positively charged conjugated polyelectrolyte has been reported by Xia *et al.*[78] (Fig. 3). In their approach, conjugated polymers induce the aggregation of Au NPs in the presence of single-stranded DNA leading to colour change; however, the particles did not aggregate in the presence of double-stranded DNA, which allows the detection of various analytes by simply changing the probe DNA (Fig. 3). More recently Niazov-Elkan *et al.*[82] reported the detection of DNA and aptamers based on the hemin/G-quadruplex complex controlled aggregation of Au NPs in the presence of cysteine. The rationale behind the mechanism is that hemin/G-quadruplex complex catalyses the oxidation of cysteine into cystine, thus inhibiting aggregation. Colorimetric detection has also been applied for the differentiation of cancerous cells from normal cells by using aptamer-labeled Au NPs by Medley *et al.*[66] In their method, Au NPs were first modified with a thiolated aptamer that has high sensitivity and selectivity toward a particular type of cancer cell, and thus, Au NPs aggregate when they are bound to target cells and appear in blue colour.

Colorimetric assays based on the aggregation of plasmonic NPs have also been applied to detection of metal ions, which is of application in biological, environmental and food safety.[16,56–58,61] For example, the detection of heavy metal ions

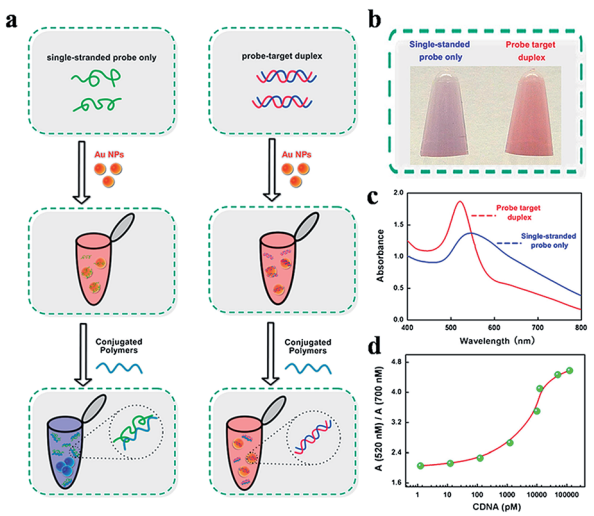

Fig. 3 Schematic representation of a colorimetric assay for DNA detection using unmodified Au NPs. (a) Scheme showing the addition of a positively charged polymer to a mixture of single-stranded DNA and Au NPs, leading to colour change from red to blue through aggregation, while no colour change is seen in the case of double-stranded DNA. (b) Photographs of colloidal solutions of Au NPs in the presence of single-stranded DNA (blue) and double-stranded DNA (red). (c) Extinction spectra of Au NPs with double-stranded and single-stranded DNA. (d) Plot of target DNA concentration *vs.* the A_{520}/A_{700} ratio, showing the possibility of determining the target concentration. (Panels a, b, c and d reproduced with permission from ref. 78.)

such as Hg^{2+} and Pb^{2+} is crucial for maintaining safe levels in drinking water. Both mercury and lead are highly harmful pollutants to the environment and human health and are circulated into humans through the food cycle. The design of Hg^{2+} assays has been mainly based on metal–ligand interactions, in which Hg^{2+} selectively induces aggregation upon complexing with ligands attached to the metal surface, causing a colour change of the solution.[16,56,57,107] Various kinds of ligands (metal ion probes) have been developed for the selective complexation with metal ions, such as thymine (T), which binds to Hg^{2+} through the coordination chemistry of T–Hg^{2+}–T complexation.[94–102] Xue *et al.*[102] reported a single-step colorimetric selective detection of Hg^{2+} using DNA–Au NP conjugates in the presence of a concentration excess of other metal ions, in which DNA contains thymine (Fig. 2b). They have shown that the Au NPs aggregate upon the addition of Hg^{2+} and complementary DNA with T–T mismatches, as shown in Fig. 1b. The DNA melting temperature can be decreased down to room temperature by increasing the number of T–T mismatches. However, the detection limit is 1 μM, thus lower than that imposed by the U.S. Environmental Protection Agency (sub-10 nM). In another report by Lee *et al.*,[95] separately conjugated Au NPs with complementary DNA strands (with T–T mismatch), which leads to aggregation upon the addition of Hg^{2+} ions. Interestingly, this approach allows Hg^{2+} quantitative detection based on the DNA melting transition curves, as the melting temperature of DNA–Au NP aggregates (reflected in changes of solution colour) depends on the amount of added Hg^{2+} ions. Lee and Mirkin demonstrated chip-based scanometric determination of mercury ions with signal amplification by Ag shell coating on DNA conjugated Au NPs, which resulted in the detection of 10 nM (2 ppb) Hg^{2+}, both in lake water and in buffer solution.[96] This method is promising for point of care detection due to its high sensitivity, easy read-out and portability. Unmodified Au NPs have also been used for the detection of Hg^{2+} ions in the presence of thrombin-binding aptamer (T rich).[101] In this method, Hg^{2+} ions interact with T-rich aptamer in such a way that it turns into a hairpin-like or quadruplex structure, leading to aggregation of the Au NPs. In addition to DNA probes, various small molecular probes have also been used for ion sensing. For instance, glutathione-functionalized Au NPs probes have been used for colorimetric Pb^{2+} detection, in which Pb^{2+} binds to glutathione molecules to induce the aggregation of Au NPs, causing colour change.[108] Recently, Du *et al.*[107] have shown that urine samples can act as probes for Hg^{2+} sensing as they include nitrogen-containing molecules, such as uric acid, which can selectively bind to Hg^{2+} and cause aggregation. The mechanism of aggregation in most of the above methods is based on metal ion induced crosslinking. In contrast, Jiang *et al.* reported Hg^{2+} sensing through a non-crosslinking aggregation mechanism.[72] In this approach, Au NPs capped with quaternary ammonium-terminated thiols were used as the probe, from which Hg^{2+} ions selectively detach the thiols, leading to NP aggregation. The detection limit of this system was improved by solar light irradiation, which causes photothermal acceleration of the Au–S bond cleavage in the presence of Hg^{2+} ions. Various other probes, such as Au NPs capped with quaternary ammonium groups, mercaptopropionic acid, tween20, lysine, or cellulose polyampholyte were also used for Hg^{2+} sensing.[72,109–112] Moreover, Au NPs based colorimetric assays have been applied for the detection of various ions, such as K^{+},[100] Cu^{2+},[113] As^{3+},[25] Ag^{+} (ref. 109) *etc.* Overall, as a result of consistent efforts from various researchers, the selectivity, sensitivity, reproducibility, and portability have been significantly improved. Wei *et al.*[62] recently demonstrated the detection and mapping of Hg contamination in water samples using a smartphone. In this method, the built-in camera module of a smartphone digitally quantified the Hg concentration by an assay based on Au NPs and T-rich aptamers, implemented in a disposable test tube. This demonstration brings the Hg detection technology from the laboratory to the real world.

In addition to DNA and ion sensing, small molecules and various biomacromolecules have also been detected *via* plasmonic nanoparticle-based colorimetric assays, including the use of molecular recognition probes, such as DNA aptamers, antigen–anitibody interactions, hydrogen bonding and supramolecular host–guest interactions. For instance, Han *et al.*[70] reported colorimetric screening of DNA-binding molecules using Au NP–DNA conjugate probes. When DNA-bound molecules were added to Au NP–DNA probes, they induced aggregation through intercross coupling and they remained aggregated at higher temperatures, while weak or non-binding molecules do not induce aggregation. Ai *et al.*[86] demonstrated the colorimetric detection of melamine in raw milk and infant formula through the design of an Au NP surface that recognizes the molecules *via* hydrogen bonding, causing the aggregation (Fig. 2c). As shown in Fig. 1c, Au NPs were functionalized with 1-(2-mercaptoethyl)-1,3,5-triazinane-2,4,6-trione, which specifically binds to melamine *via* hydrogen bonding, causing aggregation. Li *et al.*[90] developed a viologen sensor based on carboxylatopillar[5]arene stabilized Au NPs, in which viologen molecules induce NP aggregation through host–guest interactions. Colorimetric sensing has also been applied to latent fingerprinting and detection of cocaine using Au NP probes that are coupled with cocaine-specific aptamers (Fig. 2d).[91] This method is based on the identification of cocaine induced colour change by the dark field scattering technique, and the Au NP probes act as both colorimetric sensors and image contrast agents. Interestingly, LSPR-based sensing is more intense than fluorescence, optically photostable and provides high signal to noise ratios, enabling high sensitivity and spatial resolution in the imaging of fingerprints. Based on the above discussion and the examples provided in the section, it is clear that the field of colorimetric sensors for the detection of analytes has progressed well over the years and also enables the development of simple devices for detection and diagnostics. Although this colorimetric detection method may provide qualitative detection, it is still limited in providing quantitative analysis as it is difficult to distinguish the extent of aggregation based on colour changes, and it is less sensitive compared to other scattering-based detection methods, such as SERS.

4. SERS-based sensing

Raman scattering spectroscopy is a powerful technique that provides vibrational information about molecules, and thus, the Raman scattering spectrum of each molecule is a unique fingerprint. Raman scattering is the inelastic scattering of photons by a molecule, resulting from energy differences between vibrational states. However, this inelastic scattering is very weak compared to elastic scattering, and this means that Raman cross sections are typically very low. Raman spectroscopy can be performed within a wide range of excitation wavelengths (UV-IR) due to the intrinsic nature of the Raman effect, which renders Raman scattering more flexible than other techniques, such as fluorescence, in which the excitation wavelength strictly depends on the molecular properties. Therefore, it has been widely used in biology and materials science for the characterization of structure and lattice defects of various materials. However, Raman spectroscopy has limitations in the characterization of molecules at low concentrations. This limitation has been overcome after the observation of large Raman scattering from pyridine molecules adsorbed on a roughened silver surface in 1974 by Fleischmann *et al.*[114] We now know that the origin of this enhancement is related to electromagnetic field enhancements and chemical effects provided by nanostructured plasmonic metals, such as silver and gold.

Metals, such as silver and gold.[115,116] The resulting technique is called surface-enhanced Raman scattering (SERS) spectroscopy and has now been widely studied for in depth understanding and for applications in a variety of fields.[12,20,117–119] SERS has largely profited from the recent advances in colloidal nanofabrication as well as in lithographic methods and instrumentation for highly sensitive detection.[12,120,121] As a result of intense efforts by various groups, the mechanism of SERS has been well understood, which allowed the creation and characterization of highly efficient SERS substrates.[116,122] In general, the SERS activity depends on the morphology of the plasmonic nanostructures, such as their size, shape and aggregation state (dimers to multimers).[45,123–125] In particular, aggregated nanoparticles exhibit higher SERS activity than the individual components by several orders of magnitude.[45,123,124,126] Various strategies have been developed for the assembly of plasmonic nanostructures in suspension as well as on substrates to create and control hot spots for their use in various applications, such as medical diagnostics, biosensing and imaging, *etc.*[20,122,127] SERS-based sensing has also been applied for the detection of various analytes as it provides ultrahigh sensitivity down to the single molecule level, through aggregation enhanced SERS.[128] In this section, we first summarize different ways to create hot spots in plasmonic nanostructures through the controlled self-assembly of NPs, and then, we review selected strategies that have been employed for SERS-based sensing based on the aggregation of plasmonic NPs.

Controlled creation of hot spots is crucial to achieve high SERS activity through electromagnetic field enhancement. As discussed in the plasmonic coupling section, the field enhancement depends on the interparticle gap relative to particle size (Fig. 4a).[19] Plasmon coupling leads to the formation of new gap modes, and the fields associated with these new modes concentrate at the interparticle gap, leading to strong fields (Fig. 4a). Two of the most widely used methods to assemble plasmonic nanoparticles are: (1) molecular mediated self-assembly using bifunctional molecules and (2) electrostatic interactions. For example, Gandra *et al.*[129] reported plasmonic planet–satellite clusters through the self-assembly of Au NPs using the bifunctional *p*-aminothiophenol (ATP) molecule (Fig. 4b). The thiol end of ATP binds to the Au core while the $-NH_2$ group on the other end is available for noncovalent cross-linking with satellite Au NPs in such a way that the assembly can be controlled into a chain-like conformation by simply adjusting the pH (Fig. 4b). We emphasize that the chemical design of NP surfaces to obtain analyte-induced aggregation for SERS-based sensing is similar to that for colorimetric sensing. However, one should be careful in the sense that the probe molecules should be located at the interparticle gaps in order to achieve higher SERS. Kumacheva *et al.* reported a study to probe the generation of hot spots in end-to-end self-assembled Au NRs by trapping the SERS dyes within the hot spots (Fig. 4c).[65] In their study, the ends of the Au NRs were first modified with thiol-terminated polystyrene, and then, NRs were

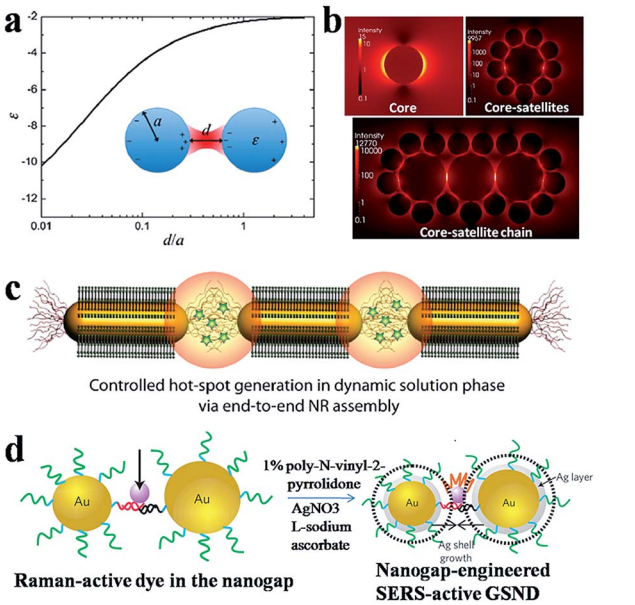

Fig. 4 Formation of hot spots: (a) permittivity ε values of sphere dimer, as a function of surface-to-surface separation *d*, normalized to the radius *a*. Charges accumulate near the gap, leading to a huge enhancement of the field. (b) Electric field distribution around the cores, core-satellites, and core-satellite chain obtained using FDTD simulations. Core-satellite structures exhibit higher enhancement over individual cores alone. (c) Formation of hot spots in between the ends of Au NRs by end-to-end assembly of NRs triggered by adding water to the colloidal suspension of thiol-terminated polystyrene functionalized Au NRs in DMF, in the presence of the Raman reporter oxazine 720. (Panels a, b, c and d reproduced with permission from ref. 19, 129, 65 and 120, respectively.)

self-assembled in the presence of SERS dyes, facilitating the trapping of dyes at the hot spots formed between the Au NRs ends (Fig. 4c). They showed that the SERS intensity increases with increasing number of nanorods in the aggregate, because of the increased number of hot spots. In another study, Lim *et al.*[120] demonstrated the creation of hot spots through the formation of NP dimers using DNA-conjugated Au NPs, in which dye-labelled DNA was used to trap the dye molecule in the hot spots (Fig. 4d). Furthermore, the interparticle gap between Au NPs present in the dimer was decreased by coating a silver shell on them, thereby facilitating single molecule detection (Fig. 4d).

Apart from ultrahigh sensitivity, an interesting feature of SERS is the capability for multiplex detection.[130] SERS-based sensing allows the simultaneous detection of several analytes by distinguishing their characteristic peaks in the spectrum, which is not possible through colorimetric methods. For instance, SERS-based sensing allowed the multiplexed detection of oligonucleotide (DNA and RNA) targets using fluorophore-labeled DNA-conjugated Au NPs (Fig. 5a).[117] SERS sensitivity was further improved by the catalytic deposition of Ag, which acts as a SERS promoter as Ag NPs exhibit higher extinction cross section than Au and lower overlap with interband transitions. Another simple process that could be applied for the creation of hot spots for efficient biosensing is based on the

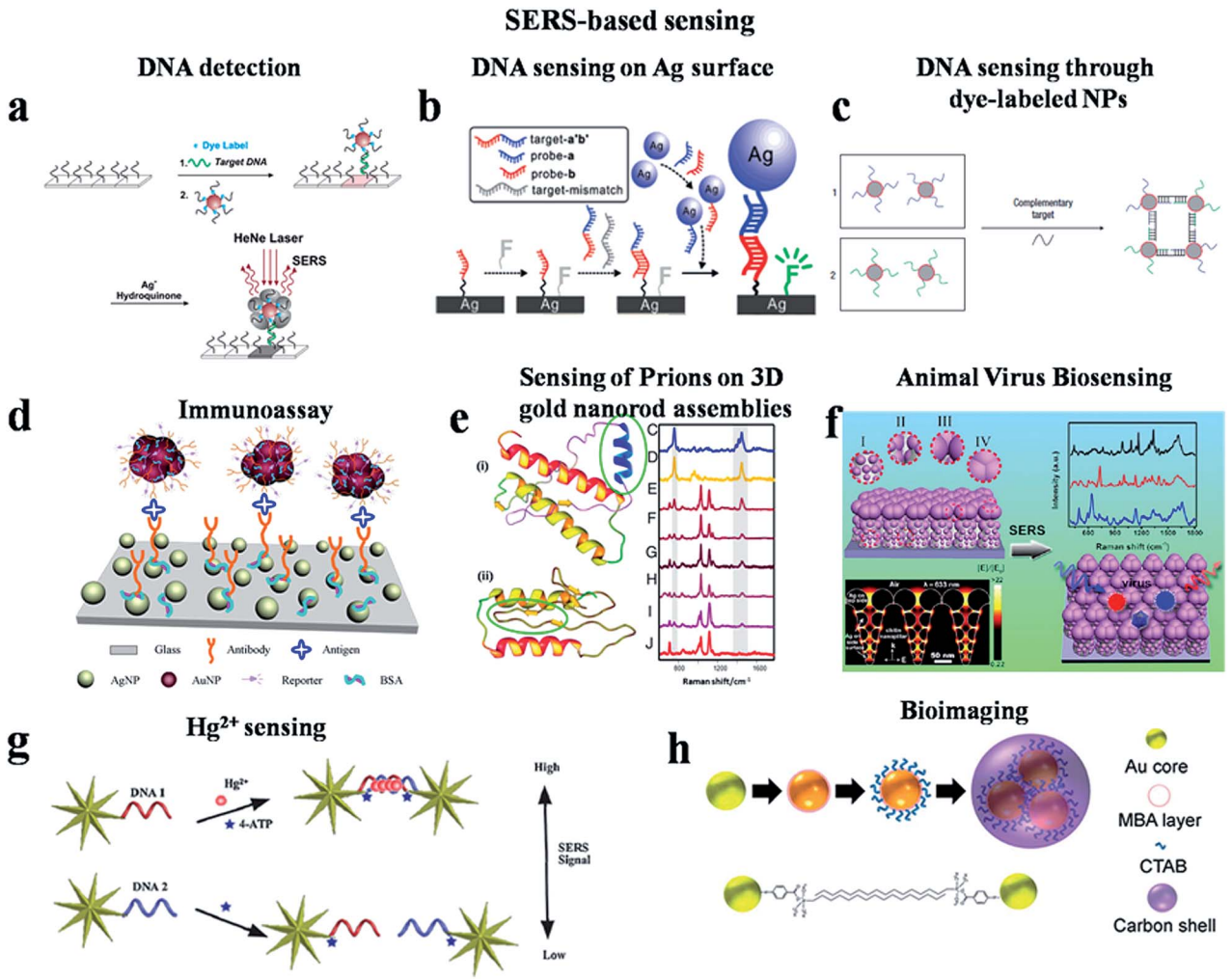

Fig. 5 SERS-based sensing: (a) schematic representation of multiplexed DNA detection using DNA conjugated Au NPs and Raman-active dyes. The catalytic reduction of Ag^+ ions on the sandwich structure causes an increase of SERS signal of the dye. (b) Schematic representation of the SERS detection of DNA on a silver surface, using Ag NPs and a Raman active probe. A target DNA strand (a'b') is captured by Ag NPs and a Raman tag (F) attached to the Ag Film, resulting in the creation of a SERS-active structure. Target DNA detection is monitored by collecting the SERS signal of the Raman tag. (c) Schematic illustration of DNA detection using dye-functionalized DNA Ag NP conjugates. (d) Strategy for a SERS-based immunoassay on glass using Raman reporter labeled Au nanoparticle aggregates through the design of the antibody–antigen structure. (e) Schematic representation of prion mutation and limit of detection for scrambled prions in bovine serum [biologically active (i) and scrambled (ii) prions]. (f) SERS-based animal virus biosensing on a 3D biomimetic SERS substrate with hierarchial nanogaps. (g) SERS based sensing of Hg^{2+} ions using T-DNA conjugated Au nanostars *via* T–Hg^{2+}–T complexation. (h) Preparation of Raman probe labeled Au NP aggregates encapsulated into a carbon shell for SERS based bioimaging (panels a, b, c, d, e, f, g and h reproduced with permission from ref. 117, 131, 132, 133, 134, 136, 138 and 140, respectively).

immobilization of plasmonic NPs on smooth metal films. For example, Moskovits *et al.* demonstrated label-free DNA sensing on a smooth Ag film by the immobilization of Ag NPs and SERS detection (Fig. 5b).[131] SERS-based DNA sensing could also be performed in solutions using DNA and dye-labelled plasmonic NPs. Graham *et al.*[132] reported a strategy to control the SERS using DNA based assembly of dye-labelled Ag NPs. In their approach, Ag NPs were first coated with a monolayer of dye, and then the particles were modified with a DNA strand to recognise the complementary strand for DNA detection (Fig. 5c). Various other bioassays include the use of Raman reporter and antibody-labelled Au NP aggregates for a highly sensitive immunoassay on Ag NPs modified glass substrates, through antibody–antigen interactions (Fig. 5d).[133] So far, the SERS sensors discussed above are based on more or less random aggregates of plasmonic NPs. However, special attention has been recently paid toward the design of SERS-based sensors comprising highly organised 3D-plasmonic supercrystals as they exhibit plasmonic antenna electrical field enhancement, causing strong SERS activity.[134] In general, such ordered NPs are separated by very small gaps depending on the surfactant molecules, and such gaps exhibit high field enhancements. Recently, our group and others reported highly organized plasmonic supercrystals made of nanorods and nanoparticles.[134,135] Alvarez-Puebla *et al.* demonstrated highly sensitive and rapid detection of scrambled prions on gold nanorod 3D supercrystals, showing that such substrates could be reused upon plasma cleaning (Fig. 5e).[134] In a related work, Shao *et al.*[136] reported the preparation of three-dimensional (3D) biomimetic SERS substrates with hierarchical nanogaps based on bioscaffold arrays of cicada wings that were coated with metal by ion-sputtering techniques (Fig. 5f). The hierarchical nanogaps could be readily controlled to generate high density of hot spots. They showed that such substrates could be used as label-free SERS substrates for the ultrasensitive detection and differentiation of animal viruses (Fig. 5f). In addition, SERS-based sensing has been widely used for the detection of metal ions, and special attention has been paid again to Hg^{2+} due to its high relavance in environment and food safety.[137,138] In general, two different approaches have been proposed for SERS-based sensing of metal ions. (1) Probing the SERS shift of the probe molecule upon selective binding to specific metal ions[139] and (2) measuring the SERS enhancement of the probe molecule upon metal ion-induced aggregation of plasmonic NPs.[138] The second method is more sensitive and exhibits higher dynamic range than the first one because of the large difference in SERS enhancement upon aggregation compared to minor Raman shifts induced by binding of the metal ion only. A recent review by Alvarez-Puebla and Liz-Marzan provides an overview on SERS-based sensing of inorganic ions through different chemical designs between ions and plasmonic NPs.[20] A recent report by Ma *et al.*[138] demonstrated mercury sensing based on the formation of SERS active gold nanostar dimers through the formation of T–Hg^{2+}–T complexes upon the addition of Hg^{2+} to DNA-conjugated Au nanostars (Fig. 5g). The design is similar to colorimetric detection as described above, but a Raman active probe molecule, such as ATP is used to probe the SERS enhancement upon aggregation depending on Hg^{2+} concentration (Fig. 5g). In addition to sensing, Raman active-labeled aggregated plasmonic NPs have also been used for SERS-based live cell imaging (Fig. 5h), as reported by Zhang *et al.*[140] Based on the above examples and the discussion, it is clear that SERS-based sensing has seen a large progress over the years. However, it still has some limitations that must be overcome before it is routinely used, such as problems associated with reproducible SERS efficiency of the plasmonic substrates.

5. Two-photon photoluminescence (TPPL)-based sensing

Two-photon induced photoluminescence (TPPL) is the emission of light from materials that are excited by simultaneous absorption of two photons of the same or different frequencies. In general, two-photon excitation has several advantages over one-photon excitation, such as high penetration depth due to infrared excitation (biologically transparent), confocal excitation, suppressed auto-fluorescence, and reduced photobleaching. Due to the wide range of applications, TPPL-based sensing and imaging has attracted significant attention in recent years. Noble metals, such as Au and Ag are generally considered as non fluorescent due to their low quantum yield. Photoluminescence (PL) from noble metals was first observed by Mooradian[141] in 1969, and it was later found by Boyd *et al.*[142] that rough metal surfaces exhibit enhanced PL. On the other hand, metal nanostructures exhibit quantum yields in the range of 10^{-4}–10^{-3}, which is 6–7 orders of magnitude higher than the emission from smooth metal surfaces.[143] This huge enhancement is also attributed to the strong local field enhancement by LSPR.[143] Although the one-photon emission quantum yield of plasmonic nanostructures is much lower than that for organic dyes, they display strong TPPL.[144,145] For instance, the TPPL intensity from a single Au NR is 58 times higher than that from a single rhodamine molecule.[145] The TPPL intensity depends on the LSPR wavelength maximum[27,37,146] and the surrounding medium,[147] and aggregated plasmonic nanoparticles exhibit enhanced TPPL over their individual counterparts, as reported by Guan *et al.*[37] The reason for this additional enhancement is related to the above described plasmon coupling, which leads to shifts of the extinction maximum into the IR, facilitating coupling with the excitation laser wavelength that leads to strong local field enhancement.[27,148] As a result, TPPL enhancement depends on the size of the plasmonic NPs, as the strength of plasmon coupling also depends on their size.[149] A recent single particle study on the TPPL enhancement of coupled Au NPs revealed that the TPPL signal increases from monomer to trimer, and the average enhancement was found to be $\sim 7.8 \times 10^3$ and $\sim 7.0 \times 10^4$ for a dimer and trimer respectively, as compared to that of individual Au NPs (Fig. 6).[27] Obviously, such a strong enhancement due to aggregation of plasmonic nanoparticles can be utilized for aggregation-based sensing (Fig. 7). Interestingly, TPPL-based sensing does not require any probe molecules like Raman tags for SERS. Plasmonic nanoparticles themselves act as TPPL probes in TPPL-

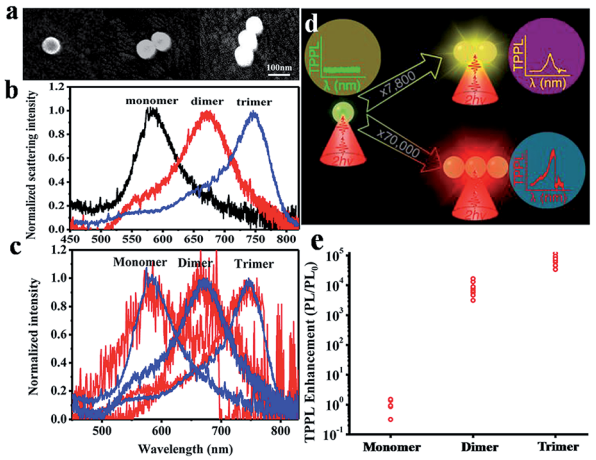

Fig. 6 (a–c) SEM images (a) scattering spectra (b) and two-photon photoluminescence spectra (c) of a monomer, dimer, and trimer. (d) Schematic representation showing the TPPL enhancement for a dimer and trimer. (e) Relative TPPL intensity as a function of the number of particles. (Panels a, b, c, d and e reproduced with permission from ref. 27.)

based sensing. One can, in principle, monitor the increase of TPPL intensity as a function of concentration of the analyte that induces nanoparticle aggregation, for quantitative detection. For example, Jiang *et al.*[150] reported label-free TPPL-based assay for sensing thrombin in serum using Ag NPs and a thrombin-binding aptamer (TBA) (Fig. 7a). In this design, TBA adsorbs on the surface of Ag NPs and helps to stabilize them, whereas, the addition of thrombin selectively binds to TBA and leads to the formation of aggregates (Fig. 7a).[150] The detection limit of the method was found to be 3.1 pM in buffer solution, which was two orders of magnitude better than the detection limit obtained from the change in UV-Vis extinction spectra. Similarly, Au nanocubes were used as TPPL probes for sensing of cysteine and glutathione, as both molecules induce the aggregation of Au NPs through electrostatic interactions at low pH (see Fig. 7b), while other non-thiolated amino acids do not induce aggregation.[151] TPPL-based sensing could also be applied to ion sensing, by measuring the TPPL of plasmonic NPs with respect to the concentration of the metal ions that induce aggregation of plasmonic NPs (Fig. 7d).[152] In addition, aggregated plasmonic spherical NPs exhibit enhanced two-photon induced singlet oxygen generation compared to isolated

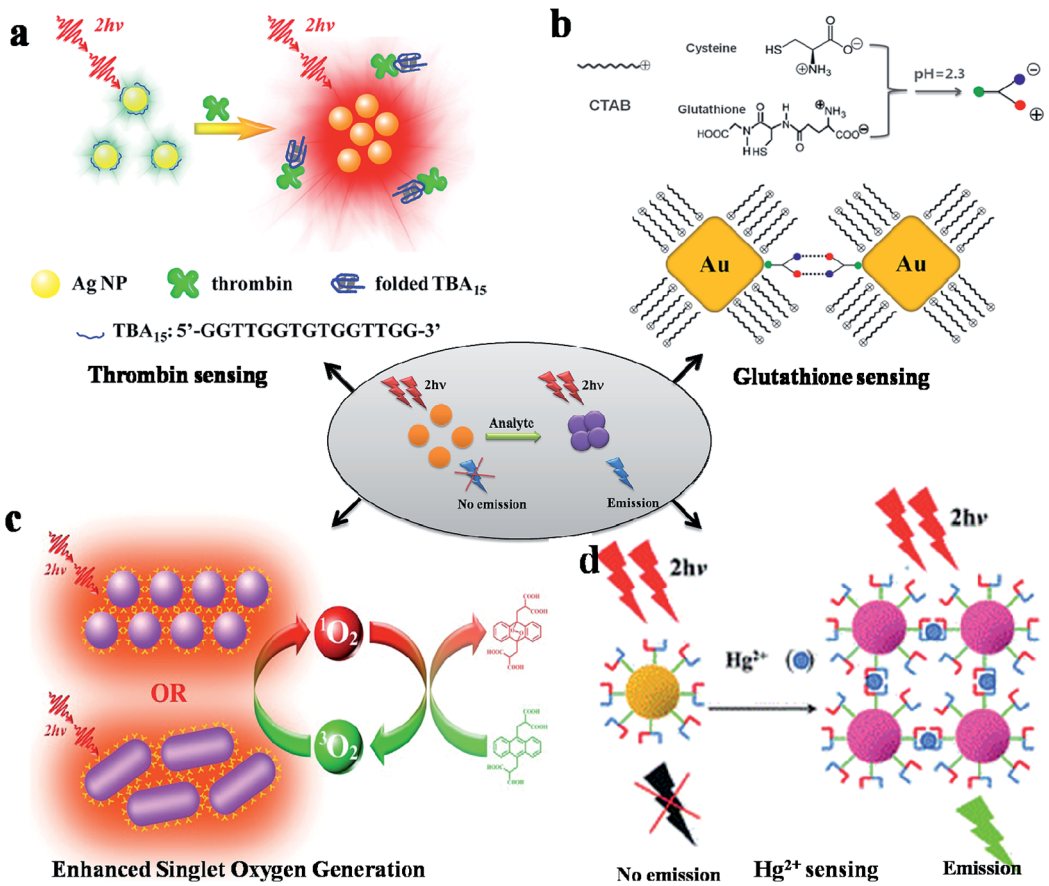

Fig. 7 TPPL-based sensing: (a) schematic representation of TPPL-based sensing of thrombin using Ag NPs and thrombin-binding aptamers. Individual Ag NPs do not exhibit TPPL, while thrombin-induced aggregated Ag NPs exhibit enhanced TPPL. (b) Strategy for TPPL based sensing of glutathione and cysteine using Au nanocubes. Glutathione and cysteine induce the aggregation of Au nanocubes *via* electrostatic interactions. (c) TPPL-based enhanced singlet oxygen generation of aggregated Au NPs. (d) Strategy for TPPL-based selective detection of Hg^{2+} ions through the aggregation of cysteine functionalized Ag NPs. (Panels a, b, c and d reproduced with permission from ref. 150, 151, 153 and 152, respectively.)

NPs, facilitating their use in two-photon photodynamic therapy as shown in Fig. 7c (in particular for Au NPs, considering their high photostability, biocompatability and inertness).[153] Overall, TPPL-based sensing is very promising for quantitative analysis. However, the applications have been greatly hindered by the requirement of expensive femtosecond lasers. Recent developments on portable and reduced cost femtosecond lasers could bring TPPL-based sensing to routine clinical diagnostic tests.

6. Dynamic light scattering and hyper-Rayleigh scattering-based sensing

In addition to the above discussed methods, the ability of plasmonic nanostructures to scatter light has also been applied for nanoplasmonic sensing, and it has become a powerful tool for ultrasensitive detection.[36,58,154–156] Plasmonic nanostructures exhibit strong, size-dependent elastic scattering, also known as Rayleigh scattering.[154,156–158] The two types of scattering based methods that have been routinely employed for sensing are dynamic light scattering (DLS) and hyper-Rayleigh scattering (HRS). DLS is a quasi-elastic scattering technique that can be used to determine the particle size distributions of small particles in colloidal solution.[159] The basic principle of DLS is that particles smaller than the wavelength of the excitation laser scatter light in all directions and the scattered intensity fluctuates over time due to the Brownian motion of particles, leading to the constructive or destructive interferences of scattered light. The average size distribution of the particles in the suspension can be obtained from the autocorrelation function of such intensity fluctuations with respect to time. DLS-based sensing is thus performed by measuring the changes in particle size distribution as a function of analyte concentration.[25,159,160] For example, Huo *et al.* demonstrated a DLS-based one-step immunoassay for cancer biomarker detection using Au nanoparticles as probes.[159] This assay is based on monitoring the antigen-induced aggregation of antibody-conjugated Au NPs through DLS. The number of particles in the aggregate, and therefore, the average size distribution increases with increasing antigen concentration, which can thus be monitored by DLS.[159] Similar assays have been applied for DNA detection as shown in Fig. 8a.[158] By mixing target DNA with two DNA-functionalized AuNP probes in solution, dimers, trimers and even larger aggregates are formed. As a result, the average size increases with the target DNA concentration.[158] Such DLS assay is highly sensitive, and it can even sense a single base pair mismatch.[158] DLS-based assays have also been applied for the detection of metal ions, such as Pb^{2+} and As^{III}, again through selective plasmonic NPs aggregation as described above.[25,157]

The other sensing technique based on light scattering is hyper-Rayleigh scattering (HRS), which is based on non-linear optical (NLO) phenomenon, in which the variation of the scattering varies in a non-linear fashion with the intensity of incident light. HRS has emerged as a powerful method for the characterization of NLO properties, such as second harmonic generation (SHG) and first hyperpolarizability of colloidal suspensions, as well as solvents.[161–164] HRS arises due to symmetry fluctuations caused by rotational changes of molecules or nanoparticles in solution. HRS is highly sensitive to particle size, shape, aggregation and surrounding environment.[161,163,165–167] For small particles ($\sim$20 nm diameter), the HRS response is mainly dominated by the dipolar contribution arising from the deviation of the particle shape from that of a perfect sphere, while for larger particles (diameter $\geq$ 80 nm), it deviates from purely dipolar and exhibits a strong quadrupolar contribution (this can be seen in the plots of polarization-dependent scattering signals).[163] In addition, the HRS intensity increases with the increase of particle size.[163,167,168] HRS is generally collected as SHG scattered signal of an excitation laser beam, and it can also be termed two-photon Rayleigh scattering or two-photon scattering.[165,169–171] HRS-based sensing has been found to be more sensitive than colorimetric methods and can resolve single base-mismatch DNA hybridization using gold nanoparticles, as reported by Ray.[155] Single stranded DNA can be adsorbed on the Au NPs surface to stabilize Au NPs, while the addition of complementary DNA desorbs the DNA and induces NPs aggregation, leading to the increase of HRS intensity. On the other hand, desorption does not happen even in the case of single base-mismatch.[155] The sensitivity of HRS was found to be 2 orders of magnitude higher than that obtained by colorimetric sensing. Similarly, sensing of specific HIV-1 virus DNA through HRS has been reported using Au nanorod probes.[172] Lu *et al.*[169] reported specific detection of breast cancer cells through colorimetric as well as HRS-based sensing using functionalized oval-shaped Au NPs (conjugated with anti-HER2 antibody and S6 RNA aptamer, see Fig. 8b). Similarly, anti-*E. coli* antibody conjugated nanorod-based identification of *E. coli* bacteria using HRS has been reported (Fig. 8c).[170] HRS-based sensing has also been applied for the detection of toxic metal ions.[26] For instance, Darbha *et al.*[26] reported the selective detection of Hg^{2+} through an HRS-based assay using mercaptopropionic acid-homocystine-2,6-pyridinedicarboxylic acid-modified gold nanoparticles. The HRS intensity was increased by 10 times upon addition of 20 ppm Hg^{2+} ions to the functionalized Au NPs, and the detection sensitivity (5 ppb) was found to be 2–3 orders of magnitude higher than that of the colorimetric method (Fig. 8d).[26] Overall, this method provides highly sensitive detection, but it also requires an expensive femtosecond laser as the excitation source. Portable designs of HRS experimental setups could help to bring this approach closer to routine sample analysis.

7. Chiroplasmonic activity-based sensing

Plasmonic nanomaterials with certain geometrical features (no possibility of superimposing mirror image) may display plasmon-related chirality, by which, they strongly affect the circular polarization of light. This phenomenon is known as chiroplasmonic activity.[28,173–178] In contrast with most chiral molecules, which exhibit weak or no optical activity in the visible region, optical activity can be achieved by exploiting the

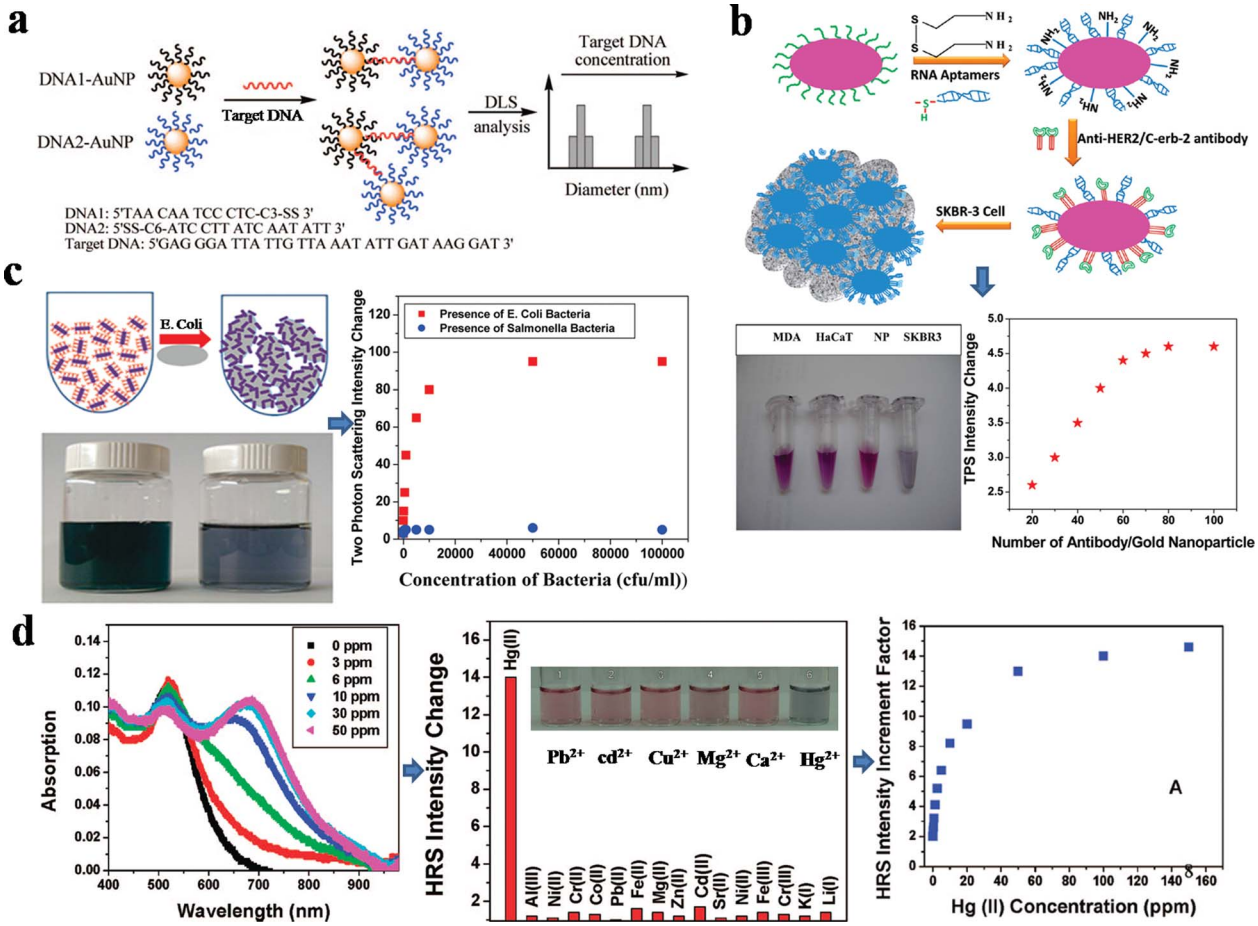

Fig. 8 DLS- and HRS-based sensing: (a) schematic representation of homogeneous DNA detection using DNA-conjugated Au NPs probes and dynamic light scattering. The average particle size in the suspension increases with the increase of target DNA concentration. (b) Schematic representation of the sensing of SK-BR-3 breast cancer cell line. The colour of NPs changes from red to blue upon binding to target cells, and the HRS intensity increases nonlinearly. (c) Anti-*E. coli* antibody conjugated nanorod-based sensing of *E. coli* bacteria. The HRS intensity increases nonlinearly with the increase of target bacteria. (d) Extinction spectra of MPA-HCys-PDCA-modified Au nanoparticles before and after the addition of Hg^{2+}; selectivity of MPA-HCys-PDCA-modified Au nanoparticles toward the detection of Hg^{2+} in the presence of other ions; quantitative determination based on the increase of HRS intensity with Hg^{2+} concentration. (Panels a, b, c and d reproduced with permission from ref. 158, 169, 170 and 26, respectively.)

chiral morphology of organic molecules coupled to the plasmonic properties of nanoparticles.[179] Therefore, the origin of the optical activity in plasmonic nanoparticles can be either due to their chiral symmetry or their interactions with chiral molecules.[28,175] This field is relatively new. However, it is quickly emerging as an important tool for applications in metamaterials and plasmonic sensing.[180–182] Initial studies on the design of chiral plasmonic nanomaterials were driven by their potential applications for metamaterials.[183,184] The fabrication of individual chiral nanoparticles is challenging, but recent demonstrations on the collective chirality of nanoparticle assemblies is a promising alternative for the construction of chiral plasmonic NPs.[28,147,185] For instance, nanometer scale chiral helices of Au NPs with tailored optical properties can be made using DNA origami as a template, as reported by Kuzyk *et al.* (Fig. 9a).[186] In this case, selective optical activity (left-handed or right-handed) in the visible was achieved by combination of the plasmonic properties of metal NPs with the chiral morphology of organic molecules (Fig. 9a).[186] Interestingly, it has been reported that chiral assemblies of anisotropic NPs, such as nanorods exhibit higher optical activity than those made of spherical nanoparticles.[28,185] Maoz *et al.*[179] showed that the chiroptical activity of biomolecules in the visible can be amplified by surface plasmons of metal nanostructures when they are placed in the proximity of the metal surface even without bonding, but the optical activity decreases with increasing separation distance. Similarly, Wang *et al.*[187] have found the amplification of the chiroptical activity of small molecules by 2 orders of magnitude when they are placed at the hot spots of plasmonic nanoparticles. Several studies have shown that assembled NPs, even dimers (homodimers or heterodimers), exhibit more intense optical activity than individual NPs, thus offering an avenue toward the design of chiroptical sensors based on controlled aggregation.[147,180,181] Although this method has not been explored with full potential, ultrasensitive chiroptical sensing of DNA[182] and metal ions[180] has been

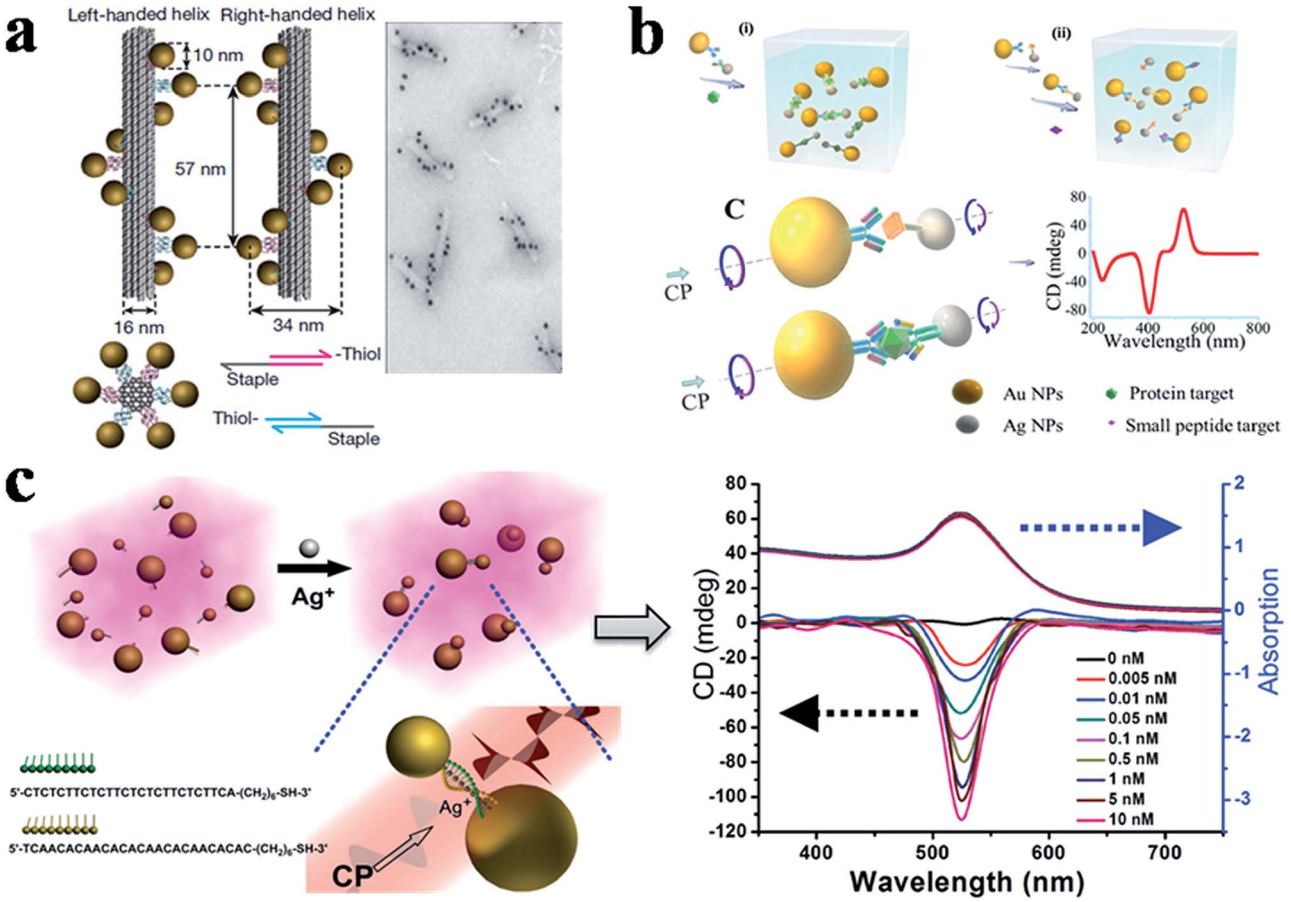

Fig. 9 (a) Schematic representation for the assembly of gold nanoparticles into helices using DNA origami template. Left- and right-handed nanohelices are formed by nine gold nanoparticles that are attached to the surface of DNA origami 24-helix bundles. (b) Schematic view of the assembly of NPs into chiral heterodimers for the detection of peptides through a competitive immunorecognition assay (i), and for detection of the large proteins *via* sandwich immunoassay mode (ii). (c) Schematic representation for the sensing of Ag^+ ions based on Cyt-Ag-Cyt recognition between cytosine-rich DNA conjugated Au (25 nm) and Ag NPs (10 nm). Circular dichroism intensity increases with the increase of Ag^+ ion concentration, while no significant changes arise in the extinction spectra. (Panels a, b and c reproduced with permission from ref. 186, 181 and 180,respectively.)

demonstrated. For example, Xu *et al.* reported ultrasensitive detection of Ag^+ ions using chiroptical assemblies of Au NPs (Fig. 8c).[180] DNA-modified Au NPs were assembled upon the addition of Ag^+ ions, leading to the formation of dimers through Cyt-Ag-Cyt recognition and causing the increase of circular dichroism (CD) intensity (Fig. 8c).[180] The limit of detection for Ag^+ sensing was reported as 2 pM. As shown in Fig. 9c, whereas the addition of Ag^+ ions to Au NPs hardly affected their extinction spectra, a linear increase of CD intensity was observed, showing the high sensitivity and quantitative nature of this method. In a recently published paper, Kotov *et al.* demonstrated attomolar DNA detection using chiral nanorod assemblies. Au NRs were assembled side-by-side with a 7–9 degree twist between the nanorod axes *via* DNA polymerase chain reaction.[182] The limit of detection for DNA using such chiral assembles was reported as 3.7 attomolar, which is much lower than that achieved using other detection methods. In addition, this method has been successfully applied for sensing toxins, microcystin-LR, and a cancer biomarker, prostate-specific antigen, using chiral heterodimers made of Au and Ag NPs (Fig. 9b).[181] The assays were based on the formation of Au–Ag heterodimers *via* biomolecular recognition, thereby monitoring the CD intensity with respect to analyte concentration (Fig. 9b). It has been proposed that the significant improvement (1 order of magnitude) in limit of detection using chiroptical sensing over other detection methods is attributed to the plasmonic enhancement of the intrinsic optical activity of biomolecules, strong CD activity in assembled NPs with twisted geometries and signal amplification due to the bisignated nature of CD bands.[181] However, only a limited amount of work has been performed on this kind of sensing methods and further study is expected in the near future.

8. Conclusions and outlook

We have broadly summarized in this feature article various strategies that have been implemented for the design of chemical interactions between analytes and the surface of metal NPs, so as to induce aggregation with a high degree of detection selectivity and sensitivity. The optical changes arising upon the

aggregation of plasmonic NPs could be detected in several ways, and we discussed different optical detection methods, such as colorimetric, SERS, TPPL, HRS and chiroptical activity, for improved detection. We hope that our discussion will motivate the integrated design of sensing devices based on plasmonic nanosensors. Although a significant amount of research has been carried out for sensing by various optical methods, each of them has its own advantages and drawbacks, and selection of the most appropriate method should be based on the requirements of a specific application. Generally, colorimetric sensing is the most suitable method for cost-effective point of care diagnostics due to the instrumentation free and portable character of the method. Portable spectrometers coupled with microarray scanners are commercially available for chip-based colorimetric diagnostics. However, colorimetric detection has some limitations as it does not provide accurate quantitative information and the detection sensitivity is lower as compared to other methods. On the other hand, SERS offers ultrasensitive, quantitative and portable detection, but the progress toward real-life applications is still limited due to problems associated with reproducibility. Other detection methods, including HRS and TPPL, also provide high sensitivity, and it would be more promising if portable spectrometers can be coupled with femtosecond lasers. In addition, the recently emerging chiroplasmonic activity-based sensing appears very promising as it provides ultrahigh sensitive detection; however, its full potential is yet to be explored. From the discussion in this feature article, it is evident that recent developments in sensor design and detection methods have greatly improved the sensitivity of optical sensors based on plasmonic nanosensors. We believe that combined efforts by scientists, engineers and medical doctors are required to develop plasmonic devices based on plasmonic nanosensors for daily life applications.

Acknowledgements

This work has been funded by the European Research Council through the Advanced Grant #267867 (PLASMAQUO). QHX thank the financial support from the National Research Foundation, Prime Minister's Office, Singapore, under its Competitive Research Programme (CRP Award no. NRF-CRP10-2012-04).

References

1 B. Brunekreef and S. T. Holgate, *Lancet*, 2002, **360**, 1233–1242.
2 P. Beaudeau, J. Schwartz and R. Levin, *Water Res.*, 2014, **52**, 188–198.
3 R. Eisert and K. Levsen, *J. Chromatogr. A*, 1996, **733**, 143–157.
4 M. E. Lindsey, M. Meyer and E. M. Thurman, *Anal. Chem.*, 2001, **73**, 4640–4646.
5 F. Dolinsek and J. Stupar, *Analyst*, 1973, **98**, 841–850.
6 G. Gilliland, S. Perrin, K. Blanchard and H. F. Bunn, *Proc. Natl. Acad. Sci. U. S. A.*, 1990, **87**, 2725–2729.
7 T. Molden, I. Kraus, F. Karlsen, H. Skomedal, J. F. Nygård and B. Hagmar, *Cancer Epidemiol., Biomarkers Prev.*, 2005, **14**, 367–372.
8 X. C. Huang, M. A. Quesada and R. A. Mathies, *Anal. Chem.*, 1992, **64**, 2149–2154.
9 O. Salata, *J. Nanobiotechnol.*, 2004, **2**, 3.
10 P. K. Jain, X. Huang, I. H. El-Sayed and M. A. El-Sayed, *Acc. Chem. Res.*, 2008, **41**, 1578–1586.
11 Y. X. Liu, X. C. Dong and P. Chen, *Chem. Soc. Rev.*, 2012, **41**, 2283–2307.
12 L. Polavarapu and L. M. Liz-Marzan, *Phys. Chem. Chem. Phys.*, 2013, **15**, 5288–5300.
13 Z. Wang and L. Ma, *Coord. Chem. Rev.*, 2009, **253**, 1607–1618.
14 N. L. Rosi and C. A. Mirkin, *Chem. Rev.*, 2005, **105**, 1547–1562.
15 S. K. Ghosh and T. Pal, *Chem. Rev.*, 2007, **107**, 4797–4862.
16 D. Vilela, M. C. Gonzalez and A. Escarpa, *Anal. Chim. Acta*, 2012, **751**, 24–43.
17 M. Lin, H. Pei, F. Yang, C. Fan and X. Zuo, *Adv. Mater.*, 2013, **25**, 3490–3496.
18 L. M. Liz-Marzán, *Langmuir*, 2005, **22**, 32–41.
19 R. Alvarez-Puebla, L. M. Liz-Marzan and F. J. G. de Abajo, *J. Phys. Chem. Lett.*, 2010, **1**, 2428–2434.
20 R. A. Alvarez-Puebla and L. M. Liz-Marzan, *Angew. Chem., Int. Ed.*, 2012, **51**, 11214–11223.
21 H. Li, M. Wang, W. Qiang, H. Hu, W. Li and D. Xu, *Analyst*, 2014, **139**, 1653–1660.
22 J. Qiu, G. Zeng, P. Pavaskar, Z. Li and S. B. Cronin, *Phys. Chem. Chem. Phys.*, 2014, **16**, 3115–3121.
23 J. N. Anker, W. P. Hall, O. Lyandres, N. C. Shah, J. Zhao and R. P. Van Duyne, *Nat. Mater.*, 2008, **7**, 442–453.
24 S. Szunerits and R. Boukherroub, *Chem. Commun.*, 2012, **48**, 8999–9010.
25 J. R. Kalluri, T. Arbneshi, S. A. Khan, A. Neely, P. Candice, B. Varisli, M. Washington, S. McAfee, B. Robinson, S. Banerjee, A. K. Singh, D. Senapati and P. C. Ray, *Angew. Chem., Int. Ed.*, 2009, **48**, 9668–9671.
26 G. K. Darbha, A. K. Singh, U. S. Rai, E. Yu, H. T. Yu and P. C. Ray, *J. Am. Chem. Soc.*, 2008, **130**, 8038–8043.
27 Z. P. Guan, N. Y. Gao, X. F. Jiang, P. Y. Yuan, F. Han and Q. H. Xu, *J. Am. Chem. Soc.*, 2013, **135**, 7272–7277.
28 A. Guerrero-Martinez, J. L. Alonso-Gomez, B. Auguie, M. M. Cid and L. M. Liz-Marzan, *Nano Today*, 2011, **6**, 381–400.
29 M. Danckwerts and L. Novotny, *Phys. Rev. Lett.*, 2007, **98**, 026104.
30 J. M. Romo-Herrera, R. A. Alvarez-Puebla and L. M. Liz-Marzan, *Nanoscale*, 2011, **3**, 1304–1315.
31 P. K. Jain and M. A. El-Sayed, *J. Phys. Chem. C*, 2008, **112**, 4954–4960.
32 K. H. Su, Q. H. Wei, X. Zhang, J. J. Mock, D. R. Smith and S. Schultz, *Nano Lett.*, 2003, **3**, 1087–1090.
33 G. Leveque and R. Quidant, *Opt. Express*, 2008, **16**, 22029–22038.
34 A. Apuzzo, M. Fevrier, R. Salas-Montiel, A. Bruyant, A. Chelnokov, G. Lerondel, B. Dagens and S. Blaize, *Nano Lett.*, 2013, **13**, 1000–1006.

35 S. A. Maier, M. L. Brongersma, P. G. Kik and H. A. Atwater, *Phys. Rev. B: Condens. Matter Mater. Phys.*, 2002, **65**, 193408.
36 P. C. Ray, *Chem. Rev.*, 2010, **110**, 5332–5365.
37 Z. P. Guan, L. Polavarapu and Q. H. Xu, *Langmuir*, 2010, **26**, 18020–18023.
38 M. C. Daniel and D. Astruc, *Chem. Rev.*, 2004, **104**, 293–346.
39 M. Grzelczak, J. Vermant, E. M. Furst and L. M. Liz-Marzán, *ACS Nano*, 2010, **4**, 3591–3605.
40 A. Guerrero-Martínez, M. Grzelczak and L. M. Liz-Marzán, *ACS Nano*, 2012, **6**, 3655–3662.
41 H. Wei and H. X. Xu, *Nanoscale*, 2013, **5**, 10794–10805.
42 B. Willingham and S. Link, *Opt. Express*, 2011, **19**, 6450–6461.
43 F. M. Huang and J. J. Baumberg, *Nano Lett.*, 2010, **10**, 1787–1792.
44 S. J. Barrow, A. M. Funston, D. E. Gomez, T. J. Davis and P. Mulvaney, *Nano Lett.*, 2011, **11**, 4180–4187.
45 N. Pazos-Perez, C. S. Wagner, J. M. Romo-Herrera, L. M. Liz-Marzán, F. J. García de Abajo, A. Wittemann, A. Fery and R. A. Alvarez-Puebla, *Angew. Chem., Int. Ed.*, 2012, **51**, 12688–12693.
46 A. S. Urban, X. Shen, Y. Wang, N. Large, H. Wang, M. W. Knight, P. Nordlander, H. Chen and N. J. Halas, *Nano Lett.*, 2013, **13**, 4399–4403.
47 J. B. Lassiter, J. Aizpurua, L. I. Hernandez, D. W. Brandl, I. Romero, S. Lal, J. H. Hafner, P. Nordlander and N. J. Halas, *Nano Lett.*, 2008, **8**, 1212–1218.
48 E. Prodan, C. Radloff, N. J. Halas and P. Nordlander, *Science*, 2003, **302**, 419–422.
49 P. Nordlander, C. Oubre, E. Prodan, K. Li and M. I. Stockman, *Nano Lett.*, 2004, **4**, 899–903.
50 S. Sheikholeslami, Y.-w. Jun, P. K. Jain and A. P. Alivisatos, *Nano Lett.*, 2010, **10**, 2655–2660.
51 A. Lombardi, M. P. Grzelczak, A. Crut, P. Maioli, I. Pastoriza-Santos, L. M. Liz-Marzán, N. Del Fatti and F. Vallée, *ACS Nano*, 2013, **7**, 2522–2531.
52 F. Hao, C. L. Nehl, J. H. Hafner and P. Nordlander, *Nano Lett.*, 2007, **7**, 729–732.
53 V. Myroshnychenko, J. Rodriguez-Fernandez, I. Pastoriza-Santos, A. M. Funston, C. Novo, P. Mulvaney, L. M. Liz-Marzan and F. J. Garcia de Abajo, *Chem. Soc. Rev.*, 2008, **37**, 1792–1805.
54 Y. Yang, S. Matsubara, M. Nogami, J. L. Shi and W. M. Huang, *Nanotechnology*, 2006, **17**, 2821–2827.
55 V. Chegel, O. Rachkov, A. Lopatynskyi, S. Ishihara, I. Yanchuk, Y. Nemoto, J. P. Hill and K. Ariga, *J. Phys. Chem. C*, 2012, **116**, 2683–2690.
56 D. Liu, Z. Wang and X. Jiang, *Nanoscale*, 2011, **3**, 1421–1433.
57 J. J. Du, L. Jiang, Q. Shao, X. G. Liu, R. S. Marks, J. Ma and X. D. Chen, *Small*, 2013, **9**, 1467–1481.
58 J. Du, B. Zhu, X. Peng and X. Chen, *Small*, 2014, DOI: 10.1002/smll.201303256.
59 D. J. de Aberasturi, J. M. Montenegro, I. R. de Larramendi, T. Rojo, T. A. Klar, R. Alvarez-Puebla, L. M. Liz-Marzan and W. J. Parak, *Chem. Mater.*, 2012, **24**, 738–745.
60 Y. W. Lin, C. C. Huang and H. T. Chang, *Analyst*, 2011, **136**, 863–871.
61 F. P. Zamborini, L. Bao and R. Dasari, *Anal. Chem.*, 2011, **84**, 541–576.
62 Q. S. Wei, R. Nagi, K. Sadeghi, S. Feng, E. Yan, S. J. Ki, R. Caire, D. Tseng and A. Ozcan, *ACS Nano*, 2014, **8**, 1121–1129.
63 L. Guerrini and D. Graham, *Chem. Soc. Rev.*, 2012, **41**, 7085–7107.
64 E. Petryayeva and U. J. Krull, *Anal. Chim. Acta*, 2011, **706**, 8–24.
65 A. Lee, G. F. S. Andrade, A. Ahmed, M. L. Souza, N. Coombs, E. Tumarkin, K. Liu, R. Gordon, A. G. Brolo and E. Kumacheva, *J. Am. Chem. Soc.*, 2011, **133**, 7563–7570.
66 C. D. Medley, J. E. Smith, Z. Tang, Y. Wu, S. Bamrungsap and W. H. Tan, *Anal. Chem.*, 2008, **80**, 1067–1072.
67 C. A. Mirkin, R. L. Letsinger, R. C. Mucic and J. J. Storhoff, *Nature*, 1996, **382**, 607–609.
68 H. Liang, X.-B. Zhang, Y. Lv, L. Gong, R. Wang, X. Zhu, R. Yang and W. Tan, *Acc. Chem. Res.*, 2014, **47**, 1891–1901.
69 Z. F. Ma, L. Tian, T. T. Wang and C. G. Wang, *Anal. Chim. Acta*, 2010, **673**, 179–184.
70 M. S. Han, A. K. R. Lytton-Jean, B. K. Oh, J. Heo and C. A. Mirkin, *Angew. Chem., Int. Ed.*, 2006, **45**, 1807–1810.
71 H. J. Parab, C. Jung, J. H. Lee and H. G. Park, *Biosens. Bioelectron.*, 2010, **26**, 667–673.
72 D. B. Liu, W. S. Qu, W. W. Chen, W. Zhang, Z. Wang and X. Y. Jiang, *Anal. Chem.*, 2010, **82**, 9606–9610.
73 L. H. Guo, Y. Xu, A. R. Ferhan, G. N. Chen and D. H. Kim, *J. Am. Chem. Soc.*, 2013, **135**, 12338–12345.
74 R. C. Jin, G. S. Wu, Z. Li, C. A. Mirkin and G. C. Schatz, *J. Am. Chem. Soc.*, 2003, **125**, 1643–1654.
75 K. Sato, K. Hosokawa and M. Maeda, *J. Am. Chem. Soc.*, 2003, **125**, 8102–8103.
76 J. J. Storhoff, R. Elghanian, R. C. Mucic, C. A. Mirkin and R. L. Letsinger, *J. Am. Chem. Soc.*, 1998, **120**, 1959–1964.
77 H. X. Li and L. Rothberg, *Proc. Natl. Acad. Sci. U. S. A.*, 2004, **101**, 14036–14039.
78 F. Xia, X. L. Zuo, R. Q. Yang, Y. Xiao, D. Kang, A. Vallee-Belisle, X. Gong, J. D. Yuen, B. B. Y. Hsu, A. J. Heeger and K. W. Plaxco, *Proc. Natl. Acad. Sci. U. S. A.*, 2010, **107**, 10837–10841.
79 R. Elghanian, J. J. Storhoff, R. C. Mucic, R. L. Letsinger and C. A. Mirkin, *Science*, 1997, **277**, 1078–1081.
80 S. J. Park, T. A. Taton and C. A. Mirkin, *Science*, 2002, **295**, 1503–1506.
81 T. A. Taton, C. A. Mirkin and R. L. Letsinger, *Science*, 2000, **289**, 1757–1760.
82 A. Niazov-Elkan, E. Golub, E. Sharon, D. Balogh and I. Willner, *Small*, 2014, **10**, 2883–2891.
83 A. H. Alhasan, D. Y. Kim, W. L. Daniel, E. Watson, J. J. Meeks, C. S. Thaxton and C. A. Mirkin, *Anal. Chem.*, 2012, **84**, 4153–4160.
84 H. X. Li and L. Rothberg, *Anal. Chem.*, 2005, **77**, 6229–6233.
85 N. T. K. Thanh and Z. Rosenzweig, *Anal. Chem.*, 2002, **74**, 1624–1628.
86 K. L. Ai, Y. L. Liu and L. H. Lu, *J. Am. Chem. Soc.*, 2009, **131**, 9496.
87 J. Deng, P. Yu, Y. Wang, L. Yang and L. Mao, *Adv. Mater.*, 2014, DOI: 10.1002/adma.201305619.

88 J. T. Huang, X. X. Yang, Q. L. Zeng and J. Wang, *Analyst*, 2013, **138**, 5296–5302.
89 H. P. Jiao, J. Chen, W. Y. Li, F. Y. Wang, H. P. Zhou, Y. X. Li and C. Yu, *ACS Appl. Mater. Interfaces*, 2014, **6**, 1979–1985.
90 H. Li, D. X. Chen, Y. L. Sun, Y. B. Zheng, L. L. Tan, P. S. Weiss and Y. W. Yang, *J. Am. Chem. Soc.*, 2013, **135**, 1570–1576.
91 K. Li, W. W. Qin, F. Li, X. C. Zhao, B. W. Jiang, K. Wang, S. H. Deng, C. H. Fan and D. Li, *Angew. Chem., Int. Ed.*, 2013, **52**, 11542–11545.
92 J. W. Liu and Y. Lu, *Angew. Chem., Int. Ed.*, 2006, **45**, 90–94.
93 H. C. Su, B. Sun, L. J. Chen, Z. N. Xu and S. Y. Ai, *Anal. Methods*, 2012, **4**, 3981–3986.
94 N. Kanayama, T. Takarada and M. Maeda, *Chem. Commun.*, 2011, **47**, 2077–2079.
95 J.-S. Lee, M. S. Han and C. A. Mirkin, *Angew. Chem., Int. Ed.*, 2007, **46**, 4093–4096.
96 J.-S. Lee and C. A. Mirkin, *Anal. Chem.*, 2008, **80**, 6805–6808.
97 D. Li, A. Wieckowska and I. Willner, *Angew. Chem., Int. Ed.*, 2008, **47**, 3927–3931.
98 L. Li, B. Li, Y. Qi and Y. Jin, *Anal. Bioanal. Chem.*, 2009, **393**, 2051–2057.
99 C.-W. Liu, C.-C. Huang and H.-T. Chang, *Langmuir*, 2008, **24**, 8346–8350.
100 L. Wang, X. Liu, X. Hu, S. Song and C. Fan, *Chem. Commun.*, 2006, 3780–3782.
101 Y. Wang, F. Yang and X. Yang, *Biosens. Bioelectron.*, 2010, **25**, 1994–1998.
102 X. Xue, F. Wang and X. Liu, *J. Am. Chem. Soc.*, 2008, **130**, 3244–3245.
103 A. P. Alivisatos, K. P. Johnsson, X. G. Peng, T. E. Wilson, C. J. Loweth, M. P. Bruchez and P. G. Schultz, *Nature*, 1996, **382**, 609–611.
104 J. J. Storhoff, A. A. Lazarides, R. C. Mucic, C. A. Mirkin, R. L. Letsinger and G. C. Schatz, *J. Am. Chem. Soc.*, 2000, **122**, 4640–4650.
105 W. A. Zhao, M. M. Ali, S. D. Aguirre, M. A. Brook and Y. F. Li, *Anal. Chem.*, 2008, **80**, 8431–8437.
106 P. Liu, X. H. Yang, S. Sun, Q. Wang, K. M. Wang, J. Huang, J. B. Liu and L. L. He, *Anal. Chem.*, 2013, **85**, 7689–7695.
107 J. J. Du, B. W. Zhu and X. D. Chen, *Small*, 2013, **9**, 4104–4111.
108 F. Chai, C. A. Wang, T. T. Wang, L. Li and Z. M. Su, *ACS Appl. Mater. Interfaces*, 2010, **2**, 1466–1470.
109 C. Y. Lin, C. J. Yu, Y. H. Lin and W. L. Tseng, *Anal. Chem.*, 2010, **82**, 6830–6837.
110 G. Sener, L. Uzun and A. Denizli, *Anal. Chem.*, 2014, **86**, 514–520.
111 C. C. Huang and H. T. Chang, *Chem. Commun.*, 2007, 1215–1217.
112 J. You, H. Z. Hu, J. P. Zhou, L. N. Zhang, Y. P. Zhang and T. Kondo, *Langmuir*, 2013, **29**, 5085–5092.
113 Y. Zhou, S. X. Wang, K. Zhang and X. Y. Jiang, *Angew. Chem., Int. Ed.*, 2008, **47**, 7454–7456.
114 M. Fleischmann, P. J. Hendra and A. J. McQuillan, *Chem. Phys. Lett.*, 1974, **26**, 163–166.
115 D. L. Jeanmaire and R. P. Van Duyne, *J. Electroanal. Chem. Interfacial Electrochem.*, 1977, **84**, 1–20.
116 M. Moskovits, *Phys. Chem. Chem. Phys.*, 2013, **15**, 5301–5311.
117 Y. W. C. Cao, R. C. Jin and C. A. Mirkin, *Science*, 2002, **297**, 1536–1540.
118 R. Kodiyath, S. T. Malak, Z. A. Combs, T. Koenig, M. A. Mahmoud, M. A. El-Sayed and V. V. Tsukruk, *J. Mater. Chem. A*, 2013, **1**, 2777–2788.
119 Z. Y. Wang, A. Bonoiu, M. Samoc, Y. P. Cui and P. N. Prasad, *Biosens. Bioelectron.*, 2008, **23**, 886–891.
120 D. K. Lim, K. S. Jeon, H. M. Kim, J. M. Nam and Y. D. Suh, *Nat. Mater.*, 2010, **9**, 60–67.
121 E. C. Le Ru and P. G. Etchegoin, *Annu. Rev. Phys. Chem.*, 2012, **63**, 65–87.
122 S. L. Kleinman, R. R. Frontiera, A.-I. Henry, J. A. Dieringer and R. P. Van Duyne, *Phys. Chem. Chem. Phys.*, 2013, **15**, 21–36.
123 K. L. Wustholz, A. I. Henry, J. M. McMahon, R. G. Freeman, N. Valley, M. E. Piotti, M. J. Natan, G. C. Schatz and R. P. Van Duyne, *J. Am. Chem. Soc.*, 2010, **132**, 10903–10910.
124 G. Chen, Y. Wang, M. X. Yang, J. Xu, S. J. Goh, M. Pan and H. Y. Chen, *J. Am. Chem. Soc.*, 2010, **132**, 3644.
125 A. Guerrero-Martinez, S. Barbosa, I. Pastoriza-Santos and L. M. Liz-Marzan, *Curr. Opin. Colloid Interface Sci.*, 2011, **16**, 118–127.
126 A. M. Schwartzberg, C. D. Grant, A. Wolcott, C. E. Talley, T. R. Huser, R. Bogomolni and J. Z. Zhang, *J. Phys. Chem. B*, 2004, **108**, 19191–19197.
127 C. Fang, A. Agarwal, K. D. Buddharaju, N. M. Khalid, S. M. Salim, E. Widjaja, M. V. Garland, N. Balasubramanian and D. L. Kwong, *Biosens. Bioelectron.*, 2008, **24**, 216–221.
128 P. G. Etchegoin and E. C. Le Ru, *Phys. Chem. Chem. Phys.*, 2008, **10**, 6079–6089.
129 N. Gandra, A. Abbas, L. M. Tian and S. Singamaneni, *Nano Lett.*, 2012, **12**, 2645–2651.
130 D. Tsoutsi, L. Guerrini, J. M. Hermida-Ramon, V. Giannini, L. M. Liz-Marzan, A. Wei and R. A. Alvarez-Puebla, *Nanoscale*, 2013, **5**, 5841–5846.
131 G. Braun, S. J. Lee, M. Dante, T. Q. Nguyen, M. Moskovits and N. Reich, *J. Am. Chem. Soc.*, 2007, **129**, 6378.
132 D. Graham, D. G. Thompson, W. E. Smith and K. Faulds, *Nat. Nanotechnol.*, 2008, **3**, 548–551.
133 C. Y. Song, Z. Y. Wang, R. H. Zhang, J. Yang, X. B. Tan and Y. P. Cui, *Biosens. Bioelectron.*, 2009, **25**, 826–831.
134 R. A. Alvarez-Puebla, A. Agarwal, P. Manna, B. P. Khanal, P. Aldeanueva-Potel, E. Carbo-Argibay, N. Pazos-Perez, L. Vigderman, E. R. Zubarev, N. A. Kotov and L. M. Liz-Marzan, *Proc. Natl. Acad. Sci. U. S. A.*, 2011, **108**, 8157–8161.
135 C. Hamon, M. Postic, E. Mazari, T. Bizien, C. Dupuis, P. Even-Hernandez, A. Jimenez, L. Courbin, C. Gosse, F. Artzner and V. Marchi-Artzner, *ACS Nano*, 2012, **6**, 4137–4146.
136 F. Shao, Z. Lu, C. Liu, H. Han, K. Chen, W. Li, Q. He, H. Peng and J. Chen, *ACS Appl. Mater. Interfaces*, 2013, **6**, 6281–6289.
137 W. Ren, C. Z. Zhu and E. K. Wang, *Nanoscale*, 2012, **4**, 5902–5909.

138 W. Ma, M. Z. Sun, L. G. Xu, L. B. Wang, H. Kuang and C. L. Xu, *Chem. Commun.*, 2013, **49**, 4989–4991.
139 D. Tsoutsi, J. M. Montenegro, F. Dommershausen, U. Koert, L. M. Liz-Marzan, W. J. Perak and R. A. Alvarez-Puebla, *ACS Nano*, 2011, **5**, 7539–7546.
140 G. Zhang, G. Qu, Y. Chen, A. Shen, W. Xie, X. Zhou and J. Hu, *J. Mater. Chem. B*, 2013, **1**, 4364–4369.
141 A. Mooradian, *Phys. Rev. Lett.*, 1969, **22**, 185–187.
142 G. T. Boyd, Z. H. Yu and Y. R. Shen, *Phys. Rev. B: Condens. Matter Mater. Phys.*, 1986, **33**, 7923–7936.
143 M. B. Mohamed, V. Volkov, S. Link and M. A. El-Sayed, *Chem. Phys. Lett.*, 2000, **317**, 517–523.
144 J. Y. Huang, W. Wang, C. J. Murphy and D. G. Cahill, *Proc. Natl. Acad. Sci. U. S. A.*, 2014, **111**, 906–911.
145 H. Wang, T. B. Huff, D. A. Zweifel, W. He, P. S. Low, A. Wei and J.-X. Cheng, *Proc. Natl. Acad. Sci. U. S. A.*, 2005, **102**, 15752–15756.
146 X. L. Liu, S. Liang, F. Nan, Z. J. Yang, X. F. Yu, L. Zhou, Z. H. Hao and Q. Q. Wang, *Nanoscale*, 2013, **5**, 5368–5374.
147 H. M. Zakaria, A. Shah, M. Konieczny, J. A. Hoffmann, A. J. Nijdam and M. E. Reeves, *Langmuir*, 2013, **29**, 7661–7673.
148 X. F. Jiang, Y. L. Pan, C. F. Jiang, T. T. Zhao, P. Y. Yuan, T. Venkatesan and Q. H. Xu, *J. Phys. Chem. Lett.*, 2013, **4**, 1634–1638.
149 F. Han, Z. P. Guan, T. S. Tan and Q. H. Xu, *ACS Appl. Mater. Interfaces*, 2012, **4**, 4746–4751.
150 C. F. Jiang, T. T. Zhao, S. Li, N. Y. Gao and Q. H. Xu, *ACS Appl. Mater. Interfaces*, 2013, **5**, 10853–10857.
151 Z. P. Guan, S. Li, P. B. S. Cheng, N. Zhou, N. Y. Gao and Q. H. Xu, *ACS Appl. Mater. Interfaces*, 2012, **4**, 5711–5716.
152 C. F. Jiang, Z. P. Guan, S. Y. R. Lim, L. Polavarapu and Q. H. Xu, *Nanoscale*, 2011, **3**, 3316–3320.
153 C. F. Jiang, T. T. Zhao, P. Y. Yuan, N. Y. Gao, Y. L. Pan, Z. P. Guan, N. Zhou and Q. H. Xu, *ACS Appl. Mater. Interfaces*, 2013, **5**, 4972–4977.
154 B. A. Du, Z. P. Li and C. H. Liu, *Angew. Chem., Int. Ed.*, 2006, **45**, 8022–8025.
155 P. C. Ray, *Angew. Chem., Int. Ed.*, 2006, **45**, 1151–1154.
156 Z. P. Li, X. R. Duan, C. H. Liu and B. A. Du, *Anal. Biochem.*, 2006, **351**, 18–25.
157 L. Beqa, A. K. Singh, S. A. Khan, D. Senapati, S. R. Arumugam and P. C. Ray, *ACS Appl. Mater. Interfaces*, 2011, **3**, 668–673.
158 Q. Dai, X. Liu, J. Coutts, L. Austin and Q. Huo, *J. Am. Chem. Soc.*, 2008, **130**, 8138–8139.
159 X. Liu, Q. Dai, L. Austin, J. Coutts, G. Knowles, J. H. Zou, H. Chen and Q. Huo, *J. Am. Chem. Soc.*, 2008, **130**, 2780.
160 X. Liu and Q. Huo, *J. Immunol. Methods*, 2009, **349**, 38–44.
161 K. Clays and A. Persoons, *Phys. Rev. Lett.*, 1991, **66**, 2980–2983.
162 Y. El Harfouch, E. Benichou, F. Bertorelle, I. Russier-Antoine, C. Jonin, N. Lascoux and P. F. Brevet, *J. Phys. Chem. C*, 2014, **118**, 609–616.
163 I. Russier-Antoine, E. Benichou, G. Bachelier, C. Jonin and P. F. Brevet, *J. Phys. Chem. C*, 2007, **111**, 9044–9048.
164 F. W. Vance, B. I. Lemon and J. T. Hupp, *J. Phys. Chem. B*, 1998, **102**, 10091–10093.
165 M. Chandra, A. M. Dowgiallo and K. L. Knappenberger, *J. Phys. Chem. C*, 2010, **114**, 19971–19978.
166 J. Nappa, G. Revillod, J. P. Abid, I. Russier-Antoine, C. Jonin, E. Benichou, H. H. Girault and P. F. Brevet, *Faraday Discuss.*, 2004, **125**, 145–156.
167 I. Russier-Antoine, J. Huang, E. Benichou, G. Bachelier, C. Jonin and P. F. Brevet, *Chem. Phys. Lett.*, 2008, **450**, 345–349.
168 J. Griffin, A. K. Singh, D. Senapati, E. Lee, K. Gaylor, J. Jones-Boone and P. C. Ray, *Small*, 2009, **5**, 839–845.
169 W. T. Lu, R. Arumugam, D. Senapati, A. K. Singh, T. Arbneshi, S. A. Khan, H. T. Yu and P. C. Ray, *ACS Nano*, 2010, **4**, 1739–1749.
170 A. K. Singh, D. Senapati, S. G. Wang, J. Griffin, A. Neely, P. Candice, K. M. Naylor, B. Varisli, J. R. Kalluri and P. C. Ray, *ACS Nano*, 2009, **3**, 1906–1912.
171 A. Neely, C. Perry, B. Varisli, A. K. Singh, T. Arbneshi, D. Senapati, J. R. Kalluri and P. C. Ray, *ACS Nano*, 2009, **3**, 2834–2840.
172 G. K. Darbha, U. S. Rai, A. K. Singh and P. C. Ray, *Chem.–Eur. J.*, 2008, **14**, 3896–3903.
173 B. Auguie, J. L. Alonso-Gomez, A. Guerrero-Martinez and L. M. Liz-Marzan, *J. Phys. Chem. Lett.*, 2011, **2**, 846–851.
174 Z. Fan, H. Zhang and A. O. Govorov, *J. Phys. Chem. C*, 2013, **117**, 14770–14777.
175 C. Noguez and I. L. Garzon, *Chem. Soc. Rev.*, 2009, **38**, 757–771.
176 W. Yan, W. Ma, H. Kuang, L. Liu, L. Wang, L. Xu and C. Xu, *J. Phys. Chem. C*, 2013, **117**, 17757–17765.
177 W. Liu, D. Liu, Z. Zhu, B. Han, Y. Gao and Z. Tang, *Nanoscale*, 2014, **6**, 4498–4502.
178 A. Querejeta-Fernández, G. Chauve, M. Methot, J. Bouchard and E. Kumacheva, *J. Am. Chem. Soc.*, 2014, **136**, 4788–4793.
179 B. M. Maoz, Y. Chaikin, A. B. Tesler, O. Bar Elli, Z. Fan, A. O. Govorov and G. Markovich, *Nano Lett.*, 2013, **13**, 1203–1209.
180 Z. Xu, L. G. Xu, L. M. Liz-Marzan, W. Ma, N. A. Kotov, L. B. Wang, H. Kuang and C. L. Xu, *Adv. Opt. Mater.*, 2013, **1**, 626–630.
181 X. L. Wu, L. G. Xu, L. Q. Liu, W. Ma, H. H. Yin, H. Kuang, L. B. Wang, C. L. Xu and N. A. Kotov, *J. Am. Chem. Soc.*, 2013, **135**, 18629–18636.
182 W. Ma, H. Kuang, L. G. Xu, L. Ding, C. L. Xu, L. B. Wang and N. A. Kotov, *Nat. Commun.*, 2013, **4**, 2689.
183 C. M. Soukoulis, S. Linden and M. Wegener, *Science*, 2007, **315**, 47–49.
184 C. M. Soukoulis and M. Wegener, *Nat. Photonics*, 2011, **5**, 523–530.
185 A. Guerrero-Martinez, B. Auguie, J. L. Alonso-Gomez, Z. Dzolic, S. Gomez-Grana, M. Zinic, M. M. Cid and L. M. Liz-Marzan, *Angew. Chem., Int. Ed.*, 2011, **50**, 5499–5503.
186 A. Kuzyk, R. Schreiber, Z. Y. Fan, G. Pardatscher, E. M. Roller, A. Hogele, F. C. Simmel, A. O. Govorov and T. Liedl, *Nature*, 2012, **483**, 311–314.
187 R.-Y. Wang, P. Wang, Y. Liu, W. Zhao, D. Zhai, X. Hong, Y. Ji, X. Wu, F. Wang, D. Zhang, W. Zhang, R. Liu and X. Zhang, *J. Phys. Chem. C*, 2014, **118**, 9690–9695.

